AdjointBackMapV2: Precise Reconstruction of Arbitrary CNN Unit's Activation via Adjoint Operators

Qing Wan*1 and Yoonsuck Choe^{†1}

¹Department of Computer Science and Engineering Texas A&M University, College Station, TX, USA, 77843

October 6, 2021

Abstract

Adjoint operators have been found to be effective in the exploration of CNN's inner workings [1]. However, the previous no-bias assumption restricted its generalization. We overcome the restriction via embedding input images into an extended normed space that includes bias in all CNN layers as part of the extended input space and propose an adjoint-operator-based algorithm that maps high-level weights back to the extended input space for reconstructing an effective hypersurface. Such hypersurface can be computed for an arbitrary unit in the CNN, and we prove that this reconstructed hypersurface, when multiplied by the original input (through an inner product), will precisely replicate the output value of each unit. We show experimental results based on the CIFAR-10 dataset that the proposed approach achieves near 0 reconstruction error.

1 Introduction

Despite many successes of Convolutional Neural Networks [CNNs] [2, 3, 4, 5, 6, 7], their inner workings remain unclear. CNN employs a series of convolution and pooling, followed by fully connected (FC) activations Thus it is hard to analyze the internal principles. There are three types of approaches to address such an opacity: (1) computing the inverse of feature maps [8, 9, 10, 11], (2) perturbation based methods [12, 13, 14, 15, 16], and (3) activation maps (heatmaps) [17, 18]. These methods estimate features that contribute most to CNN's decision. However, several limitations exist in these approaches, e.g., assumption of bijective property, analysis limited to local features, and mismatch between input dimension and the heatmap dimension. Furthermore, a recent study [19] found that many of these methods do not necessarily show the correct reasoning in CNN.

In this paper, we take a different approach. We ask a simple question of whether the linear activation value (the weighted sum right before it passes through activation functions like ReLU) of an arbitrary unit in the CNN (either in the convolution layer or in the FC layer) can be precisely reproduced by multiplying the input with a reconstructed effective hypersurface [1]. In our previous work, we showed that adjoint operators [20] could be used to derive such a hypersurface with near-zero error. However, the main limitation of our previous approach was that it did not allow bias in the CNN architecture. In this paper, we circumvent this limitation by collecting all bias values from a trained CNN and turning them into part of the input. Since this is done only when we are analyzing the trained and fixed CNN, the resulting computation is the same, whether the bias values are included in the computation in the original manner, or as part of the extended input. We test our approach on VGG7, ResNet20, and ResNet20-Fixup, using the CIFAR-10 dataset. Our results show near-zero reconstruction error for the linear activation values in all layers of these CNNs. (Note that the CNNs that we analyze do have nonlinear activation functions. Our reconstructed linear activation values can simply be passed through the nonlinear activation functions to replicate the unit's output value.)

2 Related works

Theoretical efforts to analyze CNNs include [21] and [22], where CNNs were considered over Frames, an advanced concept from Wavelet Theory. They expected to find connections between convolutional kernels and frames theory to explain CNN's inner mechanism better. A recent study [23] proposed a Neural Tangent Kernels (NTKs) to project a CNN to kernel space, in which well-explored theorems can be derived. However, vulnerabilities are inevitable in these methods.

^{*}frankqingwan@gmail.com

 $^{^\}dagger {
m choe@tamu.edu}$

Wavelet theory presumed a convolutional layer as an LTI (Linear Time-Invariant) system, which is not satisfied due to bias and nonlinear activation functions. The foundation of NTK relies on an approximation of the discrete weight update rules using continuous derivative:

$$\mathbf{w}(t+1) = \mathbf{w}(t) - \frac{\partial L(\mathbf{x}, \mathbf{y}, \mathbf{w}(t))}{\partial \mathbf{w}}, \text{ approximated as}$$

$$\frac{d\mathbf{w}(t)}{dt} = \lim_{\epsilon \to 0} \frac{\mathbf{w}(t+\epsilon) - \mathbf{w}(t)}{\epsilon} = -\frac{\partial L(\mathbf{x}, \mathbf{y}, \mathbf{w}(t))}{\partial \mathbf{w}},$$
(1)

where $\mathbf{w}(t)$ is the weights at time t, and $L(\mathbf{x}, \mathbf{y}, \mathbf{w}(t))$ is the loss function with inputs \mathbf{x} and labels \mathbf{y} . This approximation commits relative errors. Whether these errors are negligible remains questionable due to high dimensional weight matrices. Besides, the NTK regime suffers from theoretical challenges [24]. Our theory circumvents these vulnerabilities since the adjoint operator is defined via dual form [20], which entails equality relationships. Such an equality relationship guarantees that our reconstructed effective hypersurface (Section 3.3), when multiplied with the extended input (a concatenation of the input image and the collection of all biases in the CNN), will precisely replicate the linear activation value of an arbitrary unit in the CNN (both Conv layer and FC layer).

3 Model

3.1 Notations

Mathematical notations used in this paper are summarized here (the notation closely follows [25]): (1) \circledast denotes convolution; (2) $\theta_{\mathcal{X}}$ denotes the origin of the vector space \mathcal{X} ; (3) \times denotes a Cartesian product; (4) $[\mathbf{x}_n; \mathbf{x}_b]$ denotes the concatenation of two tensors, \mathbf{x}_n and \mathbf{x}_b ; (5) $\mathbf{x}[\mathbf{b}_i]$ represents an operation that retrieves the corresponding part of \mathbf{b}_i from \mathbf{x} (\mathbf{x} is a sequential concatenation of tensors $\{\mathbf{b}_i\}$); (6) $\langle \mathbf{x} | \mathbf{y} \rangle$ denotes the inner product of $\mathbf{x}, \mathbf{y} \in \mathcal{X}$; (7) \mathcal{X}^* denotes the algebraic dual of \mathcal{X} , i.e., the space of all linear functionals on \mathcal{X} ; (8) $\langle \mathbf{x}, \mathbf{x}^* \rangle$ denotes the value of a linear functional $\mathbf{x}^* \in \mathcal{X}^*$ at $\mathbf{x} \in \mathcal{X}$; and (9) $B(\mathcal{X}, \mathcal{Y})$ denotes the space of all bounded linear operators from \mathcal{X} to \mathcal{Y} .

3.2 Theory

Applying adjoint operators to a general CNN is intractable since bias is usually added right after convolution. However, this challenge can be addressed if we treat bias as another component of the input that multiplies with a unit weight (Fig.1). This way, we preserve the same computation of the CNN with bias units while maintaining our previous analysis framework for CNN without bias units.

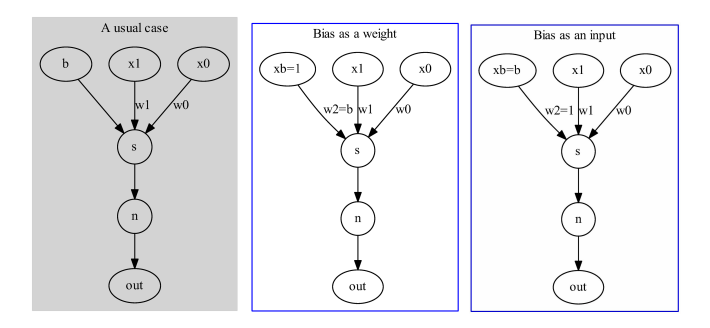


Figure 1: Two equivalent models of a trained artificial neuron. **Left**: A conventional artificial neuron with two inputs x_0, x_1 , whose weights are w_0, w_1 , respectively. Node b denotes a bias. Node b denotes a summation unit, and node b denotes an activation function. **Middle**: An equivalent model to the left. We treat the bias b as the product of the additional input b0 and a weight b1 are b2. **Right**: Another equivalent model to the left. We treat bias b3 as the third input b4 but multiplying a weight b5 are b6. Our analysis uses the last model.

Let \mathcal{X}_I and \mathcal{X}_b be two subspaces containing input images and the collected bias values, respectively. We can then construct a normed space \mathcal{X} where $\mathcal{X} = \mathcal{X}_I \times \mathcal{X}_b$. A point in this space \mathcal{X} would be a concatenation of the input image \mathbf{x}_n and the vector \mathbf{x}_b containing all bias values from the trained CNN: $[\mathbf{x}_n; \mathbf{x}_b]$ (see Fig. 2). We consider an element-wise inner product in \mathcal{X} (induces the norm on \mathcal{X}) defined as,

$$\langle [\mathbf{x}_{H \times W \times C}; \mathbf{b}_{L \times 1}] \mid [\mathbf{y}_{H \times W \times C}; \mathbf{d}_{L \times 1}] \rangle = \sum_{i=0}^{H-1} \sum_{j=0}^{W-1} \sum_{k=0}^{C-1} x_{i,j,k} y_{i,j,k} + \sum_{l=0}^{L-1} b_l d_l$$

$$= \langle \mathbf{x}_{H \times W \times C} \mid \mathbf{y}_{H \times W \times C} \rangle + \langle \mathbf{b}_{L \times 1} \mid \mathbf{d}_{L \times 1} \rangle,$$
(2)

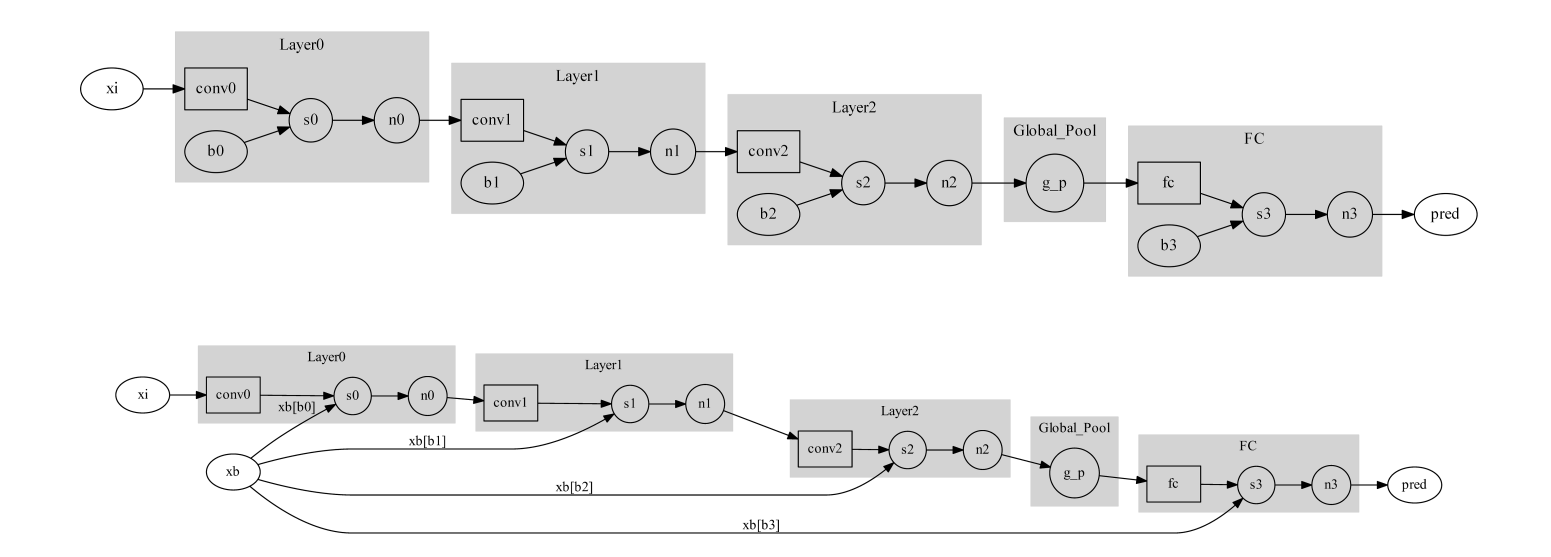


Figure 2: An equivalent model of a trained 4-layer CNN (proved in eq.(C.21)). **Top**: A CNN consists of three Conv layers, one global pooling layer, and one FC layer. Once training is finished, all parameters would be fixed. **Bottom:** We convert the trained CNN to an equivalent model. In this case, the bias values from all layers are sequentially concatenated as a big vector, $\mathbf{x}_b = [\mathbf{b}_0; \mathbf{b}_1; \mathbf{b}_2; \mathbf{b}_3]$. That vector will be fed in as an additional input tensor. Each layer picks its own bias from the \mathbf{x}_b to compute. $\mathbf{x}_b[\mathbf{b}_i]$ denotes that the corresponding part for \mathbf{b}_i will be recovered from the tensor \mathbf{x}_b . Note: \mathbf{x}_b is fixed after the CNN is trained, regardless of the input \mathbf{x}_n presented during inference.

where H, W, C means the height, width, and color channels of the input image; and L is the total number of bias values in the CNN. The first equivalence is by definition, and we use the second equivalence for tensor implementation.

Suppose \mathbf{F} is the full computation performed in a CNN's forward path from an input to an $r_1 \times r_2$ receptive field in an in-channel (in-ch) feature map (depicted by a normed space \mathcal{Y}); Bias vectors from all layers in the trained CNN are sequentially concatenated into a vector \mathbf{x}_b (Fig.2). \mathbf{F} takes the combination of an image $\mathbf{x}_n \in \mathcal{X}_I$ and the vector $\mathbf{x}_b \in \mathcal{X}_b$ as the input. Then, a kernel $\mathbf{w}_{r_1 \times r_2}$ convolving on the receptive field, $\mathbf{F}([\mathbf{x}_n; \mathbf{x}_b])$, before adding the bias vector, can be described in a dual form [20, 25],

$$c([\mathbf{x}_n; \mathbf{x}_b]) = \mathbf{F}([\mathbf{x}_n; \mathbf{x}_b]) \circledast \mathbf{w}_{r_1 \times r_2}$$

$$= \langle \mathbf{F}([\mathbf{x}_n; \mathbf{x}_b]), \mathbf{w}_{r_1 \times r_2} \rangle = \langle \mathbf{J}_{\mathbf{F}}(\mathbf{z}([\mathbf{x}_n; \mathbf{x}_b]))[\mathbf{x}_n; \mathbf{x}_b], \mathbf{w}_{r_1 \times r_2} \rangle,$$
(3)

where $c: \mathcal{X} \to \mathbb{R}$ points to a unit in the convolved feature map (before the addition of the bias); $\mathbf{J}_F: \mathcal{X} \to B(\mathcal{X}, \mathcal{Y})$ is a Jacobian operator; The third "=" holds when the CNN is activated with ReLU or Leaky ReLU, and $\mathbf{z}([\mathbf{x}_n; \mathbf{x}_b]) = k[\mathbf{x}_n; \mathbf{x}_b], k \in \mathbb{R}^+$ (proved in supplementary Appendix C). Eq.(3) implies that $\mathbf{w}_{r_1 \times r_2}$ ($\in \mathcal{Y}^*$) is a local hyperplane on \mathcal{Y} (see [1]).

For a fixed image \mathbf{x}_0 , and the vector \mathbf{x}_b constructed from a trained CNN, the Adjoint operator $\mathbf{J}_{\mathbf{F}}^*(\mathbf{z}([\mathbf{x}_0;\mathbf{x}_b]))$ will lead to the following equalities:

$$c([\mathbf{x}_{0}; \mathbf{x}_{b}]) = \langle \mathbf{J}_{\mathbf{F}}(\mathbf{z}([\mathbf{x}_{0}; \mathbf{x}_{b}]))[\mathbf{x}_{0}; \mathbf{x}_{b}], \mathbf{w}_{r_{1} \times r_{2}} \rangle = \langle [\mathbf{x}_{0}; \mathbf{x}_{b}] \mid \mathbf{J}_{\mathbf{F}}^{*}(\mathbf{z}([\mathbf{x}_{0}; \mathbf{x}_{b}]))\mathbf{w}_{r_{1} \times r_{2}} \rangle$$

$$= \langle [\mathbf{x}_{0}; \mathbf{x}_{b}] \mid \mathbf{J}_{\mathbf{F}}^{\mathsf{T}}(\mathbf{z}([\mathbf{x}_{0}; \mathbf{x}_{b}]))\mathbf{w}_{r_{1} \times r_{2}} \rangle$$

$$= \langle \mathbf{x}_{0} \mid (\mathbf{J}_{\mathbf{F}}^{\mathsf{T}}(\mathbf{z}([\mathbf{x}_{0}; \mathbf{x}_{b}]))[\mathbf{x}_{0}])\mathbf{w}_{r_{1} \times r_{2}} \rangle + \langle \mathbf{x}_{b} \mid (\mathbf{J}_{\mathbf{F}}^{\mathsf{T}}(\mathbf{z}([\mathbf{x}_{0}; \mathbf{x}_{b}]))[\mathbf{x}_{b}])\mathbf{w}_{r_{1} \times r_{2}} \rangle$$

$$(4)$$

where $\mathbf{J}_{\mathbf{F}}^{\mathsf{T}}(\mathbf{z}([\mathbf{x}_0; \mathbf{x}_b]))[\mathbf{x}_0]$, $\mathbf{J}_{\mathbf{F}}^{\mathsf{T}}(\mathbf{z}([\mathbf{x}_0; \mathbf{x}_b]))[\mathbf{x}_b]$ intends to divide the adjoint operator into two parts (two operators) in response to $\mathbf{x}_0, \mathbf{x}_b$; The second "=" and the last "=" holds thanks to the Riesz Representation theorem [25] and the distributive property of a linear operator, respectively. Riesz Representation also contributes to the unification of \mathcal{X} and \mathcal{X}^* or \mathcal{Y} and \mathcal{Y}^* . Therefore, we have $\mathbf{w}_{r_1 \times r_2} \in \mathcal{Y}$ and $\mathbf{J}_{\mathbf{F}}^*(\mathbf{z}([\mathbf{x}_0; \mathbf{x}_b])) \in B(\mathcal{Y}, \mathcal{X})$. The two operators (Eq.(5)) will map a convolution kernel from a convolutional layer or a weight vector from the FC layer all the way back to the image subspace \mathcal{X}_I and the bias subspace \mathcal{X}_b , respectively.

$$\mathbf{J}_{\mathbf{F}}^{*}(\mathbf{z}([\mathbf{x}_{0}; \mathbf{x}_{b}]))[\mathbf{x}_{0}]\mathbf{w}_{r_{1}\times r_{2}} \in \mathcal{X}_{I},
\mathbf{J}_{\mathbf{F}}^{*}(\mathbf{z}([\mathbf{x}_{0}; \mathbf{x}_{b}]))[\mathbf{x}_{b}]\mathbf{w}_{r_{1}\times r_{2}} \in \mathcal{X}_{b}.$$
(5)

The two will jointly reconstruct an effective hypersurface representing all decision hyperplanes forward from the input to an arbitrary unit of the out-ch feature map or a class value of the FC layer. We name this method AdjointBackMapV2 and observe these three fundamental properties:

- 1. The mapping, $\mathbf{J}_{\mathbf{F}}(\mathbf{z}([\mathbf{x}_n; \mathbf{x}_b]))$ (i.e., $(\mathbf{J}_{\mathbf{F}}) \circ (\mathbf{z}) : \mathcal{X} \to B(\mathcal{X}, \mathcal{Y})$), is not linear since $\exists \mathbf{x}_1, \mathbf{x}_2 \in \mathcal{X}_I$, such that, $\mathbf{J}_{\mathbf{F}}(\mathbf{z}(\alpha[\mathbf{x}_1, \mathbf{x}_b] + \beta[\mathbf{x}_2, \mathbf{x}_b])) \neq \alpha \mathbf{J}_{\mathbf{F}}(\mathbf{z}([\mathbf{x}_1, \mathbf{x}_b])) + \beta \mathbf{J}_{\mathbf{F}}(\mathbf{z}([\mathbf{x}_2, \mathbf{x}_b]))$ for two scalars, α, β ;
- 2. Eq.(5) suggests a single effective hyperplane will have two components instead of two effective hyperplanes;
- 3. A connection to the theory of [1] comes from Eq.(4) that, if all bias were zeroed out from the CNN's layers, the extended norm space \mathcal{X} would shrink to the \mathcal{X}_I that is identical to the input space in [1].

3.3 Algorithm

Layers considered for analysis Generally, the AdjointBackMapV2 is designed to work on two types of layers inside a CNN. Fig.3 illustrates our principles in detail. (1) Any kernel of a convolutional layer (except the kernels from the first layer, which has already been elements in \mathcal{X}^*) can be projected back to a joint space \mathcal{X} concatenating input images and bias vectors. This back-mapped pattern determines the pixel's linear activation value (the weighted sum) of an out-channel (out-ch) feature map; (2) Any weight vector of the FC layer can be projected back to space \mathcal{X} as well. This back-mapped pattern determines the linear activation value of classification output.

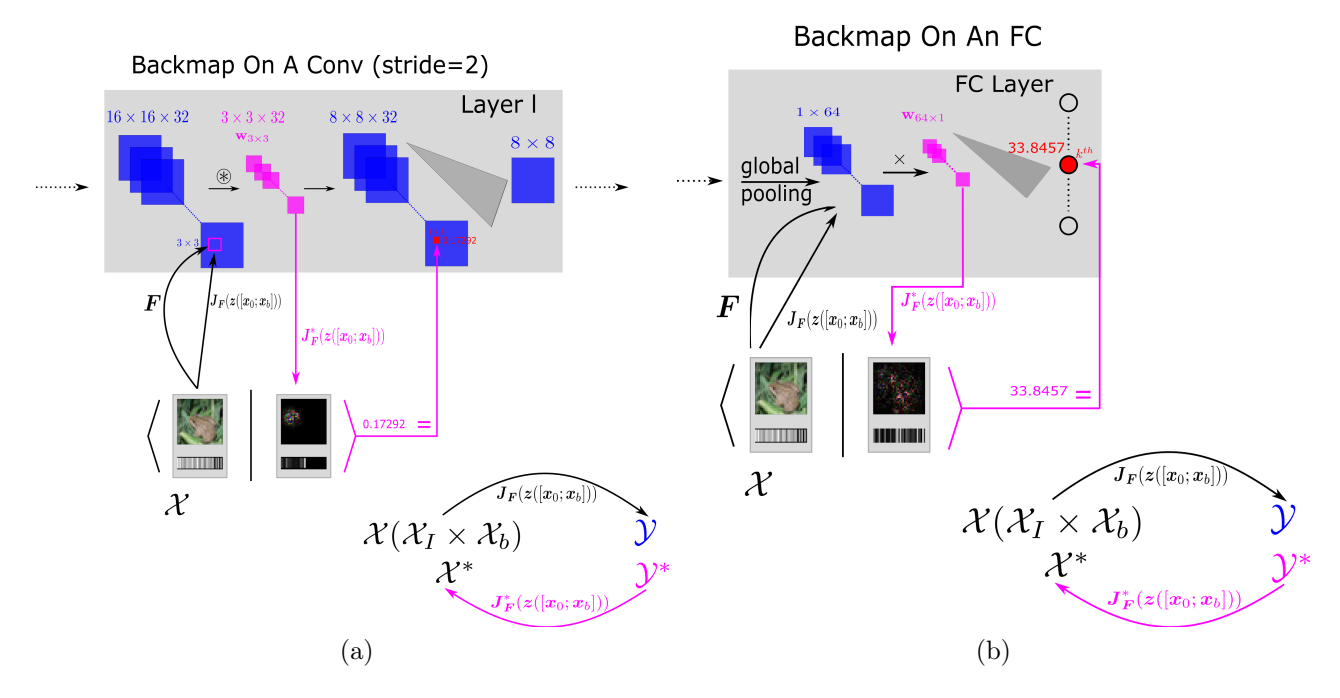


Figure 3: Principles of AdjointBackMapV2. Our reconstruction method applies to units in (a) Conv layers, and (b) FC layers. We color elements from the same normed space identically. The normed \mathcal{X} is an input space that involves two embedded subspaces \mathcal{X}_I and \mathcal{X}_b . Considering a fixed image $\mathbf{x}_0 \in \mathcal{X}_I$ and the trained bias values in the CNN (a fixed $\mathbf{x}_b \in \mathcal{X}_b$), \mathbf{F} depicts the CNN's forward computation path from the input end to an $r_1 \times r_2$ receptive field in an in-ch feature map or the global pooling layer. Its adjoint operator, $\mathbf{J}_{\mathbf{F}}^*(\mathbf{z}([\mathbf{x}_0; \mathbf{x}_b]))$, projects the corresponding kernel or weights back to the input space \mathcal{X} . Riesz Representation unites $\mathcal{X}, \mathcal{X}^*$ or $\mathcal{Y}, \mathcal{Y}^*$, together. The " $\langle \cdot | \cdot \rangle$ " notation represents a dot-product defined in Eq.(2). The symbol "=" means that a dot-product between the extended input and the reconstructed effective hyperplane is equal to the unit's linear activation value (the weighted sum) of a convolved feature map or an FC layer's output value, as long as the CNN is activated with ReLU or Leaky ReLU.

Premise Our algorithm's necessary condition is the third equality ("=") between the left and right-hand sides in Eq.(3). Alternatively, any CNN neuron holding Eq.(C.28) should satisfy our requirements. The proof in supplementary Appendix C reveals that any piecewise linear operations attached to a CNN's layers will not affect the equality. Thus, usual architectural techniques like shortcuts/concatenations/multiple receptive-field kernels' sizes fall under the scope of our analysis. In that case, most variants of CNNs activated with ReLUs or Leaky ReLUs could be analyzed with our method. Our method may not be appropriate for investigating a network activated with functions whose derivatives are not piecewise constants, such as tanh. In general, we insist that numerical precision should be considered when studying a CNN's inner workings (i.e., the method should reproduce the output values precisely), while existing methods of shaping a kernel as a filter did not achieve this.

Incorporating batch normalization Usually, bias serves CNNs in two operational modes: (1) Acting as trainable parameters attached after convolution operations; And (2) used as moving parameters that track channel-wise average batch values (BN, batch normalization [26]). The first one has a similar network topology as Fig.2, which is trivial for our theory to accommodate. The batch normalization case is more complex than the first. We will discuss it in detail in the supplementary Appendix D.

Five reconstruction modes (RMs) Our AdjointBackMapV2 approach provides five reconstruction modes (RMs) to reconstruct the effective hypersurface, depending on the location of the unit in the CNN, and on the convolution operation's variant: RM0 will project from the FC layer, and the remaining four ($RM4 \sim RM1$) will project from a convolutional layer. Generally, two factors will distinguish one RM from another:

- 1. Whether to separate the kernels in-channel-wise for mapping:
- 2. Whether to split the strides down for mapping.

All RMs and their algebraic relationships between the forward and backward paths are illustrated in Fig.4. For a more concrete discussion, we use the following setup. Suppose a CNN with Leaky ReLU as activation function has been trained on CIFAR-10. It takes a $32 \times 32 \times 3$ (height × width × channels) RGB image \mathbf{x}_n to predict 10 classes. Its l^{th} Conv layer has kernels $\mathbf{w}_{l,3\times3\times32\times64}$ (h × w × in-chs × out-chs) convolving on $16 \times 16 \times 32$ in-ch feature maps with convolution stride = 2 and padding = "SAME" [27]. The implementation of 2-D convolution [27] states: a kernel $\mathbf{w}_{3\times3}$ only convolves on its corresponding 16×16 in-ch feature map through 8×8 (a stride move s ranges from 0 to 63). Then, all 32 convolved feature maps are added together in-channel-wise (in-ch summation) as an 8×8 out-ch feature map that will be subsequently added to the bias. Thus, the l^{th} layer is supposed to produce an $8 \times 8 \times 64$ out-ch feature map. Besides, it may have global pooling [28] (g-p) applied right after activated feature maps, before entering the FC layer.

(RM4) Separations are performed on both in-ch kernels and training strides. In this case, a kernel will be individually mapped via $\mathbf{H}_{l,s,j,i}^{Adj}$, composed of $\mathbf{H}_{l,s,j,i}^{Adj,I}$ and $\mathbf{H}_{l,s,j,i}^{Adj,b}$, to space \mathcal{X} , defined as:

$$\mathbf{H}_{l,s,j,i}^{Adj,I}(\mathbf{z}([\mathbf{x}_{n};\mathbf{x}_{b}])) = (\mathbf{J}_{\mathbf{F}_{l-1,s,j,i}}^{*}(\mathbf{z}([\mathbf{x}_{n};\mathbf{x}_{b}]))[\mathbf{x}_{n}])\mathbf{w}_{l,3\times3,s,j,i},
\mathbf{H}_{l,s,j,i}^{Adj,b}(\mathbf{z}([\mathbf{x}_{n};\mathbf{x}_{b}])) = (\mathbf{J}_{\mathbf{F}_{l-1,s,j,i}}^{*}(\mathbf{z}([\mathbf{x}_{n};\mathbf{x}_{b}]))[\mathbf{x}_{b}])\mathbf{w}_{l,3\times3,s,j,i}
s \in \{0,1,...,63\}, j \in \{0,1,...,31\}, i \in \{0,1,...,63\},$$
(6)

where $\mathbf{F}_{l-1,s,j,i}$ denotes the forward path from the input end to an in-ch 3×3 receptive field that will be convolved to the (j,i) out-ch unit at the stride moves s. $\mathbf{H}_{l,s,j,i}^{Adj}$ reflects how the local kernel behaves on the combined image and bias input when the stride moves. $\langle [\mathbf{x}_n; \mathbf{x}_b] \mid [\mathbf{H}_{l,s,j,i}^{Adj,\mathbf{z}}(\mathbf{z}([\mathbf{x}_n; \mathbf{x}_b])); \mathbf{H}_{l,s,j,i}^{Adj,b}(\mathbf{z}([\mathbf{x}_n; \mathbf{x}_b]))] \rangle$ should be equal to the pixel value before the in-ch summation. Fig.4(a) (or Fig.3(a)) shows the details.

(RM3) Separations are taken on in-ch kernels only. Moreover, the effective hypersurfaces from an individual kernel sum together pixel-wise to reconstruct an effective hypersurface, $\mathbf{H}_{l,j,i}^{Adj}$. That effective hypersurface describes the local kernel's weighting on the input space, considering all stride moves merged. In other words, it reveals how a feature sum could be generated from space \mathcal{X} 's perspective, when an in-channel convolved feature map is pooling globally (Fig.4(b)), i.e.,

$$\sum_{s=0}^{63} \mathbf{F}_{l-1,s,j,i}([\mathbf{x}_n, \mathbf{x}_b]) \otimes \mathbf{w}_{l,3\times3,s,j,i} = \langle [\mathbf{x}_n; \mathbf{x}_b], \mathbf{H}_{l,j,i}^{Adj}(\mathbf{z}([\mathbf{x}_n; \mathbf{x}_b])) \rangle$$

$$= \langle \mathbf{x}_n, \sum_{s=0}^{63} (\mathbf{J}_{\mathbf{F}_{l-1,s,j,i}}^*(\mathbf{z}([\mathbf{x}_n; \mathbf{x}_b]))[\mathbf{x}_n]) \mathbf{w}_{l,3\times3,s,j,i} \rangle + \langle \mathbf{x}_b, \sum_{s=0}^{63} (\mathbf{J}_{\mathbf{F}_{l-1,s,j,i}}^*(\mathbf{z}([\mathbf{x}_n; \mathbf{x}_b]))[\mathbf{x}_b]) \mathbf{w}_{l,3\times3,s,j,i} \rangle,$$

$$(7)$$

where the distributive law and linearity in dual space support the last "=". Thus, $\mathbf{H}_{l,j,i}^{Adj}$ is composed of two operators: $\mathbf{H}_{l,j,i}^{Adj,I}$ and $\mathbf{H}_{l,j,i}^{Adj,b}$,

$$\mathbf{H}_{l,j,i}^{Adj,I}(\mathbf{z}([\mathbf{x}_n; \mathbf{x}_b])) = \sum_{s=0}^{63} \mathbf{H}_{l,s,j,i}^{Adj,I}(\mathbf{z}([\mathbf{x}_n; \mathbf{x}_b])),$$

$$\mathbf{H}_{l,j,i}^{Adj,b}(\mathbf{z}([\mathbf{x}_n; \mathbf{x}_b])) = \sum_{s=0}^{63} \mathbf{H}_{l,s,j,i}^{Adj,b}(\mathbf{z}([\mathbf{x}_n; \mathbf{x}_b])).$$
(8)

The relationship to RM4 is evident from Eq.(8).

(RM2) Separations are carried out along the training strides only. The kernels' back maps will merge in-channel-wise to reconstruct an effective hypersurface $\mathbf{H}_{l,s,i}^{Adj}$ that determines the unit's linear activation value of an out-ch feature map

(Fig.4(c)). Its two operators, $\mathbf{H}_{l,s,i}^{Adj,I}$ and $\mathbf{H}_{l,s,i}^{Adj,b}$, are defined below,

$$\mathbf{H}_{l,s,i}^{Adj,I}(\mathbf{z}([\mathbf{x}_n; \mathbf{x}_b])) = \sum_{j=0}^{31} \mathbf{H}_{l,s,j,i}^{Adj,I}(\mathbf{z}([\mathbf{x}_n; \mathbf{x}_b])),$$

$$\mathbf{H}_{l,s,i}^{Adj,b}(\mathbf{z}([\mathbf{x}_n; \mathbf{x}_b])) = \sum_{j=0}^{31} \mathbf{H}_{l,s,j,i}^{Adj,b}(\mathbf{z}([\mathbf{x}_n; \mathbf{x}_b])).$$
(9)

Eq.(9) also relates RM2 to RM4.

(RM1) Neither of the separations are performed for mapping. Then, a reconstruction will be conducted using $\mathbf{H}_{l,i}^{Adj}$ that determines the linear activation value of the feature maps for the global-pooling layer (Fig.4(d)). Its two parts, $\mathbf{H}_{l,i}^{Adj,I}$ and $\mathbf{H}_{l,i}^{Adj,b}$, and their relationships to RM3, RM2 are summarized below.

$$\mathbf{H}_{l,i}^{Adj,I}(\mathbf{z}([\mathbf{x}_n; \mathbf{x}_b])) = \sum_{j=0}^{31} \mathbf{H}_{l,j,i}^{Adj,I}(\mathbf{z}([\mathbf{x}_n; \mathbf{x}_b])) = \sum_{s=0}^{63} \mathbf{H}_{l,s,i}^{Adj,I}(\mathbf{z}([\mathbf{x}_n; \mathbf{x}_b]))$$

$$\mathbf{H}_{l,i}^{Adj,b}(\mathbf{z}([\mathbf{x}_n; \mathbf{x}_b])) = \sum_{j=0}^{31} \mathbf{H}_{l,j,i}^{Adj,b}(\mathbf{z}([\mathbf{x}_n; \mathbf{x}_b])) = \sum_{s=0}^{63} \mathbf{H}_{l,s,i}^{Adj,b}(\mathbf{z}([\mathbf{x}_n; \mathbf{x}_b])).$$

$$(10)$$

(RM0) Mapping an FC weight vector \mathbf{w}_k is independent of the factors that govern the convolution operation. An effective hypersurface $\mathbf{H}_k^{Adj}(\mathbf{z}([\mathbf{x}_n;\mathbf{x}_b]))$ reconstructed in this way represents the whole decision process towards a predicted value for the k^{th} class (Fig.3(b)). \mathbf{H}_k^{Adj} consists of two operators $\mathbf{H}_k^{Adj,I}$ and $\mathbf{H}_k^{Adj,b}$ ($k \in \{0,1,..,9\}$) as well.

$$\mathbf{H}_{k}^{Adj,I}(\mathbf{z}([\mathbf{x}_{n};\mathbf{x}_{b}])) = (\mathbf{J}_{\mathbf{F}_{g_{-p}}}^{*}(\mathbf{z}([\mathbf{x}_{n};\mathbf{x}_{b}]))[\mathbf{x}_{n}])\mathbf{w}_{k},
\mathbf{H}_{k}^{Adj,b}(\mathbf{z}([\mathbf{x}_{n};\mathbf{x}_{b}])) = (\mathbf{J}_{\mathbf{F}_{g_{-p}}}^{*}(\mathbf{z}([\mathbf{x}_{n};\mathbf{x}_{b}]))[\mathbf{x}_{b}])\mathbf{w}_{k}.$$
(11)

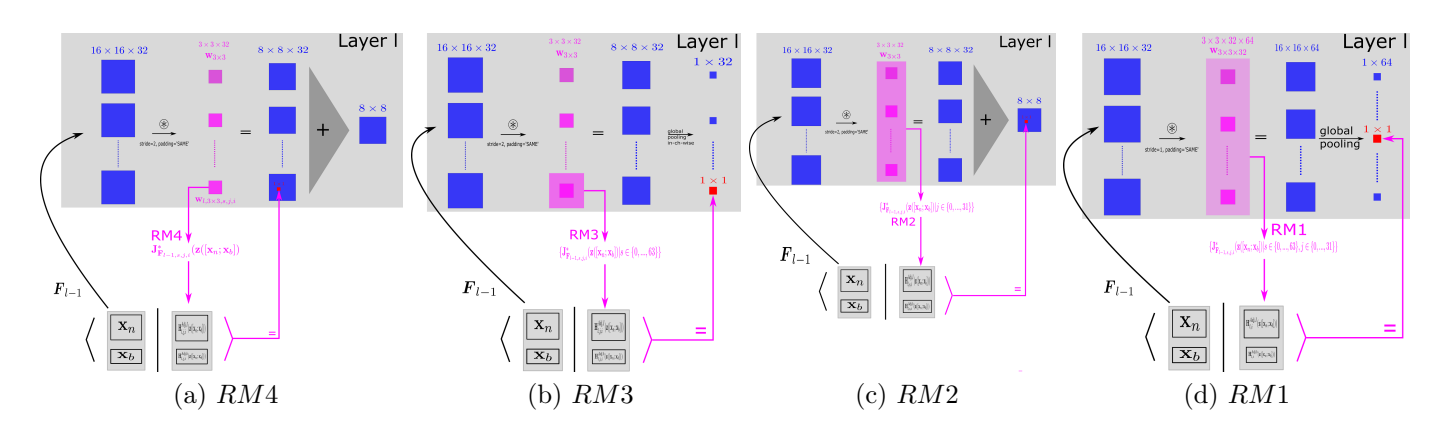


Figure 4: Two factors determine four RMs involved in the Conv layers. (a) RM4: Separate mappings along with training strides and in-channel kernels; (b) RM3: Separate mappings along with in-channel kernels only; (c) RM2: Separate mappings along with convolution strides only; (d) RM1: Neither are separated. The usage of colors is similar to Fig.3. An oversized pink mask in either (b) or (d) denotes an effective hypersurface reconstructed in response to a stride-wise summation of the convolved feature map. The symbol " $\langle \cdot | \cdot \rangle$ " refers to the inner product defined in Eq.(2).

Implementation The algorithm is summarized in supplementary Appendix E.

4 Experiments and results

We presented our theory in the previous section (proof in the supplementary Appendix C). This section will further verify our theory experimentally. As we mentioned in Section 3.3, there are two operational modes of CNN's bias: (1) Conventional parameters trained for adjusting the channels' output, and (2) auxiliary parameters trained for batch normalization. We select three CNN models that involve either of these two operational modes. Also, these three models include both supported activation functions: ReLU and Leaky ReLU. Generally, we will verify the nontrivial Eq.(3) on every layer of the CNN (except the first layer, the reason has been discussed in Section 3.3). Hardware and software used for this verification are listed in supplementary Appendix B.

4.1 Pre-trained CNNs and their equivalent topologies

We elaborate training/validation/test settings on all models. We also discuss how we convert a trained CNN model to a reduced version using eq.(D.30).

Dataset and augmentation We used the CIFAR-10 ([29]; RGB images; Resolution: 32×32 ; Pixel value range: [0, 1]; Two sets included: 50k training, 10k test). Training was conducted on 45k of the 50k set (randomly selected), and validation is conducted on the remaining 5k. The test is performed on the 10k set. Data augmentation methods are employed in training. An input image sequentially goes through the random left or right flipping, the random adjustments of saturation(within [0,2.0])/contrast(within [0.4,1.6])/brightness(within 0.5), random cropping to $32 \times 32 \times 3$ after resizing to $36 \times 36 \times 3$.

Models and their reductions We use three standard models: VGG7 [5] with 7 ReLUs, ResNet20 ([6], code: [30]) with 20 Leaky ReLUs, and ResNet20-Fixup (The Right most one in Figure 1 in [31], an input image requires normalization on its RGB channels using mean [0.4914, 0.4822, 0.4465] and variance [0.2023, 0.1994, 0.2010], code: [32]) with the Fixup initialization and 20 ReLUs. The first two use the second bias operational mode (batch normalization), and the last one uses the first bias operational mode (conventional bias mode). Their parameters are listed in supplementary table 3, 5, and 6, respectively. VGG7 and ResNet20 are trained with BN layers first. After training, we extract $\mathbf{w}, \gamma, \beta, \mu, \sigma^2$ (supplementary eq.(D.29)) to compute and collect the corresponding \mathbf{w}' and \mathbf{b}' with supplementary eq.(D.30), layer by layer. Then, we rebuild every architectural layer with its \mathbf{w}' and \mathbf{b}' to construct a new model (fig.5). Similarly, ResNet20-Fixup is trained first; We extract all kernels and biases after training. We rebuilt every layer (we merge any convolutional layer having a multiplier, check the third column of table 6) to construct an equivalent model. We verify that every rebuilt model achieves identical accuracy as its pre-trained version. We employ the rebuilt ones for experiments.

Loss function, accuracy, training, validation, test We use a summation of the kernels' regularization on the L_1 norm and the cross-entropy on a prediction's softmax as the loss function. We use Top-1 accuracy. Training, validation, and test are conducted on an RTX 3090 GPU. All three CNN models are trained with Gradient Descent optimizers (GD) on a batch size of 100. Table 1 shows additional details. We train on the 45k samples every epoch and validate the trained model on the 5k samples every two epochs. If a higher validation accuracy is reached, the trained model will be saved. We test with the 10k test samples.

Table 1: Details for training VGG7/ResNet20/ResNet20-Fixup. "0.01, [0,299]" denotes the learning rate (lr) 0.01 during the training interval, maintained during the 0^{th} to the 299^{th} training epoch. Note that the classification accuracies are modest at best, but since our thrust is primarily theoretical, we did not attempt to further fine-tune the default hyperparameters in the available open-source implementations that we used.

Models/lr intervals	1^{st} interval	2^{nd} interval	3^{rd} interval	Total	Test Acc
VGG7	0.01, [0, 299]	0.002, [300, 399]	0.0005, [400, 500]	501	89.5%
ResNet20	0.01, [0, 99]	0.001, [100, 149]	0.0002, [150, 200]	201	91.6%
ResNet20-Fixup	0.002, [0, 79]	0.001, [80, 119]	0.0005, [120, 150]	151	91.2%

4.2 Verifying Eq.(3) on the CNN models

As we mentioned, we will experimentally verify that $\mathbf{z}([\mathbf{x}_n; \mathbf{x}_b]) = \frac{[\mathbf{x}_n; \mathbf{x}_b]}{8}$ achieves the equality in Eq.(3).

We verify it on two types of layers: every Conv layer, and the FC layer. In other words, we verify that the linear activation value of an out-ch feature map's unit or the FC layer's output unit, computed through the original trained CNN, should be equal to the dot-product between the input $[\mathbf{x}_n; \mathbf{x}_b]$ and the reconstructed effective hyperplane $\mathbf{H}^{Adj}(\frac{[\mathbf{x}_n; \mathbf{x}_b]}{8})$. The verification can be described with two equations, Eq.(12) (Conv) and Eq.(13) (FC). Principles of the verification are illustrated using a symbol '=" in these previous figures: Fig.4(c) (Conv), and Fig.3(b) (FC).

$$c_{l,s,i} = \underbrace{\mathbf{F}_{l-1,s,i}([\mathbf{x}_n; \mathbf{x}_b]) \circledast \mathbf{w}_{l,s,i}}_{\text{Original CNN activation (Conv)}} = \hat{c}_{l,s,i} = \underbrace{\langle \mathbf{x}_n \mid \mathbf{H}_{l,s,i}^{Adj,I}([\frac{[\mathbf{x}_n; \mathbf{x}_b]}{8})\rangle + \langle \mathbf{x}_b \mid \mathbf{H}_{l,s,i}^{Adj,b}([\frac{[\mathbf{x}_n; \mathbf{x}_b]}{8})\rangle,}_{\text{Reconstructed Conv unit activation using Adjoint}}$$
(12)

$$c_{fc,k} = \underbrace{\mathbf{F}_{fc,k}([\mathbf{x}_n; \mathbf{x}_b])}_{\text{Original CNN activation (FC)}} = \hat{c}_{fc,k} = \underbrace{\langle \mathbf{x}_n \mid \mathbf{H}_k^{Adj,I}(\frac{[\mathbf{x}_n; \mathbf{x}_b]}{8}) \rangle + \langle \mathbf{x}_b \mid \mathbf{H}_k^{Adj,b}(\frac{[\mathbf{x}_n; \mathbf{x}_b]}{8}) \rangle}_{\text{Reconstructed FC unit activation using Adjoint}},$$
(13)

where $c_{l,s,i}$ and $c_{fc,k}$ are true values (correspond to the left-hand side of the third "=" in Eq.(3)) while $\hat{c}_{l,s,i}$ and $\hat{c}_{fc,k}$ are approximated ones (correspond to the right-hand side of the third "=" in Eq.(3)); $c_{l,s,i}$ labels a pixel at the stride moves s, in the i^{th} out-ch feature map of the l^{th} Conv layer (i.e., a unit of \mathbf{c}_l); $c_{fc,k}$ labels the k^{th} entry in the \mathbf{c}_{fc} , from the FC layer, for activating a specific class unit. In detail, for an image \mathbf{x}_n , a dot-product should be verified to replicate a unit's linear activation value from the Conv or the FC layer, and this verification should go through pixels/predicted classes' values of all layers except for the first one (which has been explained in Section 3.3); Also, RM2 is entangled with RM4, RM3, RM1 (Eq.(6) \sim (10)), which implies verifying RM2 is equivalent to verifying $RM4 \sim RM1$. Since TensorFlow uses FP32 datatype (single precision) to compute a decimal, rounding errors are inevitable and result in a fractional mismatch between \mathbf{c}_l and $\hat{\mathbf{c}}_l$ due to different computation paths. We measure relative errors ϵ for evaluating the approximations, i.e.,

$$\epsilon_l = \frac{\hat{\mathbf{c}}_l - \mathbf{c}_l}{\mathbf{c}_{l,\neq 0}},\tag{14}$$

where l is either the Conv layer index or the FC layer; $\mathbf{c}_{l,\neq 0}$ substitutes all zeros inside \mathbf{c}_l with the smallest positive float of FP32 to avoid any divide by zero exception.

4.3 Results

We verify our CNN's unit reconstruction approach on VGG7/ResNet20/ResNet20-Fixup with the 10k test samples. For a CNN model, relative errors ϵ_l are collected layer by layer over the 10k samples. All relative errors are shown as histograms in the supplementary fig.6, 7, and 8 (supplementary Appendix F). VGG7 has 6 histograms (5 convs + 1 FC), and ResNet20/ResNet20-Fixup each have 19 histograms (18 convs + 1 FC). Percentages of units with reconstruction error $\epsilon_l \leq 1\%$ collected from all models' layers are listed in Table 2 below. In summary, all three models show that over 99.97% of the units have relative reconstruction errors $\leq 1\%$. These results experimentally validate that $\mathbf{z}([\mathbf{x}_n; \mathbf{x}_b]) = \frac{[\mathbf{x}_n; \mathbf{x}_b]}{8}$, given in Eq.(3).

Therefore, the soundness of our theory is confirmed.

Table 2: Percentages (%) of units with reconstruction error $\epsilon_l \leq 1\%$ collected from all layers (involved in verification experiments) of VGG7/ResNet20/ResNet20-Fixup over the CIFAR-10 test set (10k samples). N/A indicates that the layer does not exist (VGG7 has only 6 layers, and its Conv0 is not valid in our analysis scope).

ϵ_l / % / Models	VGG7	ResNet20	ResNet20-Fixup
ϵ_1	99.9987	99.9999	99.9972
ϵ_2	99.9978	99.9994	99.9992
ϵ_3	99.9985	99.999	99.9993
ϵ_4	99.9935	99.9977	99.9989
ϵ_5	99.9933	99.9974	99.9974
ϵ_6	99.991 (FC)	99.9919	99.9975
ϵ_7	N/A	99.9835	99.9914
ϵ_8	N/A	99.9839	99.9946
ϵ_9	N/A	99.986	99.9954
ϵ_{10}	N/A	99.9877	99.9959
ϵ_{11}	N/A	99.9835	99.9953
ϵ_{12}	N/A	99.9871	99.9955
ϵ_{13}	N/A	99.9807	99.9935
ϵ_{14}	N/A	99.9808	99.9935
ϵ_{15}	N/A	99.978	99.9943
ϵ_{16}	N/A	99.9781	99.9934
ϵ_{17}	N/A	99.9764	99.9929
ϵ_{18}	N/A	99.978	99.9927
ϵ_{19}	N/A	99.989 (FC)	99.992 (FC)

5 Conclusions

In this work, we presented an analysis framework for a general CNN architecture, where each units' linear activation value can be precisely replicated using a simple inner product between the input and the effective hypersurface reconstructed through adjoint operators. Such reconstructed hypersurfaces can not only replicate the activation value of the CNN, but in itself, it can serve as a window into the inner workings of the CNN. The main contribution of this work is in the extension

of our previous adjoint-operator-based reconstruction approach to include bias, and by extension, support analysis of CNN models that include batch normalization. Our empirical validation gave robust results (\sim 99.9% of units with less than 1% reconstruction error). In the future, we intend to study the intrinsic properties of the reconstructed hypersurfaces to gain deeper insights into the hidden mechanisms of CNNs.

6 Acknowledgements

We would like to thank Siu Wun Cheung (Department of Mathematics, Texas A&M University) for helpful discussion.

References

- [1] Qing Wan and Yoonsuck Choe. Adjointbackmap: Reconstructing effective decision hypersurfaces from cnn layers using adjoint operators. arXiv preprint arXiv:2012.09020, 2020.
- [2] John Nickolls, Ian Buck, Michael Garland, and Kevin Skadron. Scalable parallel programming with cuda: Is cuda the parallel programming model that application developers have been waiting for? *Queue*, 6(2):40–53, 2008.
- [3] Sharan Chetlur, Cliff Woolley, Philippe Vandermersch, Jonathan Cohen, John Tran, Bryan Catanzaro, and Evan Shelhamer. cudnn: Efficient primitives for deep learning. arXiv preprint arXiv:1410.0759, 2014.
- [4] Alex Krizhevsky, Ilya Sutskever, and Geoffrey E Hinton. Imagenet classification with deep convolutional neural networks. Advances in neural information processing systems, 25:1097–1105, 2012.
- [5] Karen Simonyan and Andrew Zisserman. Very deep convolutional networks for large-scale image recognition. arXiv preprint arXiv:1409.1556, 2014.
- [6] Kaiming He, Xiangyu Zhang, Shaoqing Ren, and Jian Sun. Deep residual learning for image recognition. In *Proceedings* of the IEEE conference on computer vision and pattern recognition, pages 770–778, 2016.
- [7] Barret Zoph, Vijay Vasudevan, Jonathon Shlens, and Quoc V Le. Learning transferable architectures for scalable image recognition. In *Proceedings of the IEEE conference on computer vision and pattern recognition*, pages 8697–8710, 2018.
- [8] Matthew D Zeiler and Rob Fergus. Visualizing and understanding convolutional networks. In *European conference on computer vision*, pages 818–833. Springer, 2014.
- [9] Jost Tobias Springenberg, Alexey Dosovitskiy, Thomas Brox, and Martin Riedmiller. Striving for simplicity: The all convolutional net. arXiv preprint arXiv:1412.6806, 2014.
- [10] Wojciech Samek, Grégoire Montavon, Alexander Binder, Sebastian Lapuschkin, and Klaus-Robert Müller. Interpreting the predictions of complex ml models by layer-wise relevance propagation. arXiv preprint arXiv:1611.08191, 2016.
- [11] Alexey Dosovitskiy and Thomas Brox. Inverting visual representations with convolutional networks. In *Proceedings of the IEEE conference on computer vision and pattern recognition*, pages 4829–4837, 2016.
- [12] David Baehrens, Timon Schroeter, Stefan Harmeling, Motoaki Kawanabe, Katja Hansen, and Klaus-Robert Müller. How to explain individual classification decisions. *The Journal of Machine Learning Research*, 11:1803–1831, 2010.
- [13] Karen Simonyan, Andrea Vedaldi, and Andrew Zisserman. Deep inside convolutional networks: Visualising image classification models and saliency maps. arXiv preprint arXiv:1312.6034, 2013.
- [14] Marco Tulio Ribeiro, Sameer Singh, and Carlos Guestrin. "why should i trust you?" explaining the predictions of any classifier. In *Proceedings of the 22nd ACM SIGKDD international conference on knowledge discovery and data mining*, pages 1135–1144, 2016.
- [15] Pang Wei Koh and Percy Liang. Understanding black-box predictions via influence functions. In *International Conference on Machine Learning*, pages 1885–1894. PMLR, 2017.
- [16] Been Kim, Martin Wattenberg, Justin Gilmer, Carrie Cai, James Wexler, Fernanda Viegas, et al. Interpretability beyond feature attribution: Quantitative testing with concept activation vectors (tcav). In *International conference* on machine learning, pages 2668–2677. PMLR, 2018.

- [17] Bolei Zhou, Aditya Khosla, Agata Lapedriza, Aude Oliva, and Antonio Torralba. Learning deep features for discriminative localization. In *Proceedings of the IEEE conference on computer vision and pattern recognition*, pages 2921–2929, 2016.
- [18] Ramprasaath R Selvaraju, Michael Cogswell, Abhishek Das, Ramakrishna Vedantam, Devi Parikh, and Dhruv Batra. Grad-cam: Visual explanations from deep networks via gradient-based localization. In *Proceedings of the IEEE international conference on computer vision*, pages 618–626, 2017.
- [19] Akshayvarun Subramanya, Vipin Pillai, and Hamed Pirsiavash. Fooling network interpretation in image classification. In *Proceedings of the IEEE/CVF International Conference on Computer Vision*, pages 2020–2029, 2019.
- [20] Stefan Banach. Theory of linear operations. Elsevier, 1987.
- [21] Thomas Wiatowski and Helmut Bölcskei. A mathematical theory of deep convolutional neural networks for feature extraction. *IEEE Transactions on Information Theory*, 64(3):1845–1866, 2017.
- [22] Qiang Qiu, Xiuyuan Cheng, Guillermo Sapiro, et al. Dcfnet: Deep neural network with decomposed convolutional filters. In *International Conference on Machine Learning*, pages 4198–4207. PMLR, 2018.
- [23] Arthur Jacot, Franck Gabriel, and Clément Hongler. Neural tangent kernel: Convergence and generalization in neural networks. arXiv preprint arXiv:1806.07572, 2018.
- [24] Soufiane Hayou, Arnaud Doucet, and Judith Rousseau. Mean-field behaviour of neural tangent kernel for deep neural networks. arXiv preprint arXiv:1905.13654, 2019.
- [25] David G Luenberger. Optimization by vector space methods. John Wiley & Sons, 1997.
- [26] Sergey Ioffe. Batch renormalization: Towards reducing minibatch dependence in batch-normalized models. arXiv preprint arXiv:1702.03275, 2017.
- [27] Martín Abadi, Paul Barham, Jianmin Chen, Zhifeng Chen, Andy Davis, Jeffrey Dean, Matthieu Devin, Sanjay Ghemawat, Geoffrey Irving, Michael Isard, et al. Tensorflow: A system for large-scale machine learning. In 12th {USENIX} symposium on operating systems design and implementation ({OSDI} 16), pages 265–283, 2016.
- [28] Min Lin, Qiang Chen, and Shuicheng Yan. Network in network. arXiv preprint arXiv:1312.4400, 2013.
- [29] Alex Krizhevsky, Geoffrey Hinton, et al. Learning multiple layers of features from tiny images. 2009.
- [30] Google Official GitHub. Tensorflow official models. https://github.com/tensorflow/models, Nov, 2018 (accessed).
- [31] Hongyi Zhang, Yann N Dauphin, and Tengyu Ma. Fixup initialization: Residual learning without normalization. arXiv preprint arXiv:1901.09321, 2019.
- [32] Hongyi Zhang. Fixup initialization implementation in pytorch. https://github.com/hongyi-zhang/Fixup, Nov, 2020 (accessed).

Supplementary Materials

Appendix A Notations

We will use the following notations.

- 1. "Eq" refers to an equation in the main paper;
- 2. "eq" refers to an equation in the appendix;
- 3. "Table" refers to a table in the main paper;
- 4. "table" refers to a table in the appendix;
- 5. "Fig" refers to a figure in the main paper;
- 6. "fig" refers to a figure in the appendix;
- 7. "algorithm" refers to an algorithm in the appendix.

Appendix B Hardware and software for verification experiments

Verification experiments (fig.6, 7, 8) were conducted on Intel 10920X (VGG7/ResNet20) and 9940X (ResNet20-Fixup) CPUs. Both set up ran TensorFlow 1.15.4 with AVX-2, AVX-512, and FMA3 instruction sets enabled (built from source). Computing results for fig.6, fig.7, and fig.8 consumed roughly 25 hours, 778 hours, and 625 hours, respectively.

Appendix C Proof of Eq.(3)

We show $\mathbf{z}([\mathbf{x}_n; \mathbf{x}_b]) = k[\mathbf{x}_n; \mathbf{x}_b](k \in \mathbb{R}^+)$ achieves the third equality ("=") in Eq.(3) if the units in the CNN are activated with ReLU or Leaky ReLU activation function. We also generalize this conclusion to any piecewise linear activation function when k = 1 is applied.

Notations and concepts Let $\mathbf{N}: \mathcal{X}_I \to \mathbb{R}^K$ be a CNN (without the last softmax layer) with L convolutional layers, and $\mathbb{R}^{H \times W \times C}$ be an instance of input image space \mathcal{X}_I where H, W, C denote height, width, color channels of an image. Suppose $\mathbf{x}_n \in \mathbb{R}^{H \times W \times C}$ is an input image; The l^{th} layer has convolutional kernels $\mathbf{w}_{r_{l,1} \times r_{l,2} \times c_{l,in} \times c_{l,out}}$ and bias \mathbf{b}_l ($0 \le l \le L - 1$). We use $\mathbf{c}_l(\mathbf{x}_n)$ to represent the convolved feature maps with a bias vector added in the l^{th} layer, and $\hat{\mathbf{c}}_l(\mathbf{x}_n)$ the vectorization of $\mathbf{c}_l(\mathbf{x}_n)$, where $\hat{\cdot}$ is a vectorization operator. We use $\mathbf{p}_l(\mathbf{x}_n)$ to represent the activated feature maps in the l^{th} layer (the layer has an activation σ_l)), and $\hat{\mathbf{p}}_l(\mathbf{x}_n)$ the vectorization of $\mathbf{p}_l(\mathbf{x}_n)$. Their shapes are $\mathbf{c}_l, \mathbf{p}_l \in \mathbb{R}^{h_l \times w_l \times c_{l,in}}$ and $\hat{\mathbf{c}}_l, \hat{\mathbf{p}}_l, \mathbf{b}_l \in \mathbb{R}^{m_l}$ where $m_l = h_l w_l c_{l,in}$. Specifically, $(h_{-1}, w_{-1}, c_{-1,in}) = (H, W, C)$, $m_{-1} = HWC$, and $\hat{\mathbf{p}}_{-1}(\mathbf{x}_n) = \hat{\mathbf{c}}_{-1}(\mathbf{x}_n) = \hat{\mathbf{x}}_i \in \mathbb{R}^{m_{-1}}$. Then, their relationships can be described as below:

$$\mathbf{c}_{l}(\mathbf{x}_{n}) = \mathbf{p}_{l-1}(\mathbf{x}_{n}) \otimes \mathbf{w}_{r_{l,1} \times r_{l,2} \times c_{l,in} \times c_{l,out}} + \mathbf{b}_{l}$$

$$= \hat{\mathbf{c}}_{l}(\mathbf{x}_{n}) = \mathbf{A}_{l}(\hat{\mathbf{p}}_{l-1}(\mathbf{x}_{n})) = \mathbf{W}_{l}(\hat{\mathbf{p}}_{l-1}(\mathbf{x}_{n})) + \mathbf{b}_{l},$$

$$\mathbf{p}_{l}(\mathbf{x}_{n}) = \sigma_{l}(\mathbf{c}_{l}(\mathbf{x}_{n})) = \sigma_{l}(\hat{\mathbf{c}}_{l}(\mathbf{x}_{n})) = \hat{\mathbf{p}}_{l}(\mathbf{x}_{n}),$$
(C.15)

where $\mathbf{W}_l \in \mathbb{R}^{m_t \times m_{t-1}}$ is the matrix representation for the layer's convolution, and \mathbf{A}_l is an affine operator that describes the convolution and bias addition. The neural network parameters, $\{(\mathbf{W}_l, \mathbf{b}_l)\}_{l=0}^{l=L-1}$ defines the composition of convolutions, average/max poolings (average pooling is equivalent to convolving with $r_{l,1} \times r_{l,2}$ -sized averaging kernels, and max pooling is equivalent to convolving with $r_{l,1} \times r_{l,2}$ -sized one-hot kernels), and batch normalizations inside the CNN \mathbf{N} . We formalize the pixel-wise activation function σ_l as following,

$$\sigma_l(c) = \max(c, 0) + \gamma_l \min(c, 0), \forall c \in \mathbb{R}, \tag{C.16}$$

where the leakiness $\gamma_l = 0$ implies σ_l being ReLU, and $0 < \gamma_l < 1$ implies σ_l being Leaky ReLU. The convolutional layers are terminated at l = L - 1, and the overall final output of the CNN $\mathbf{N}(\mathbf{x}_l) \in \mathbb{R}^K$ is given by,

$$\mathbf{c}_{L}(\mathbf{x}_{n}) = \hat{\mathbf{c}}_{L}(\mathbf{x}_{n}) = \mathbf{A}_{L}(\hat{\mathbf{c}}_{L-1}(\mathbf{x}_{n})) = \mathbf{W}_{L}\hat{\mathbf{c}}_{L-1}(\mathbf{x}_{n}) + \mathbf{b}_{L}$$

$$\mathbf{N}(\mathbf{x}_{n}) = \hat{\mathbf{p}}_{L}(\mathbf{x}_{n}) = \sigma_{L}(\hat{\mathbf{c}}_{L}(\mathbf{x}_{n})).$$
(C.17)

Combining the above, we have (o denotes the operator composition),

$$\mathbf{N}(\mathbf{x}_n) = (\sigma_L \circ \mathbf{A}_L \circ \sigma_{L-1} \circ \mathbf{A}_{L-1} \circ \dots \sigma_1 \circ \mathbf{A}_1 \circ \sigma_0 \circ \mathbf{A}_0)(\hat{\mathbf{p}}_{-1}(\mathbf{x}_n)). \tag{C.18}$$

Representation of the equivalent topology in Fig.2 We use $M = \sum_{l=0}^{L} m_l$, which is equal to \mathbf{x}_b 's dimensions. For $0 \le l \le L$, we introduce a restriction operator $\mathbf{r}_l : \mathbb{R}^M \to \mathbb{R}^{m_l}$, by

$$\mathbf{r}_l(\mathbf{v}_b) = \mathbf{y}_l, \forall \mathbf{v}_b = [\mathbf{y}_0; \mathbf{y}_1; ...; \mathbf{y}_L] \in \mathbb{R}^M \text{ with } \mathbf{y}_l \in \mathbb{R}^{m_l}.$$
 (C.19)

Note that \mathbf{v}_b is a variable vector who has an instance \mathbf{x}_b . Then, we define a sequence of auxiliary mappings $\{\mathscr{C}_l\}_{l=0}^{l=L-1}$ by the recurrence relation: for $[\hat{\mathbf{x}}_i;\mathbf{v}_b] \in \mathbb{R}^{m_{-1}} \times \mathbb{R}^M$,

$$\mathscr{C}_{0}([\hat{\mathbf{x}}_{i}; \mathbf{v}_{b}]) = \mathbf{W}_{0}\hat{\mathbf{x}}_{i} + \mathbf{r}_{0}(\mathbf{v}_{b}),$$

$$\mathscr{C}_{l}([\hat{\mathbf{x}}_{i}; \mathbf{v}_{b}]) = \mathbf{W}_{l}(\sigma_{l-1}(\mathcal{C}_{l-1}([\hat{\mathbf{x}}_{i}; \mathbf{v}_{b}]))) + \mathbf{r}_{l}(\mathbf{v}_{b}), 0 \leq l \leq L - 1,$$

$$\mathscr{C}_{L}([\hat{\mathbf{x}}_{i}; \mathbf{v}_{b}]) = \mathbf{W}_{L}(\sigma_{L-1}(\mathcal{C}_{L-1}([\hat{\mathbf{x}}_{i}; \mathbf{v}_{b}]))) + \mathbf{r}_{L}(\mathbf{v}_{b}).$$
(C.20)

Combining eq.(C.15) and (C.17), we get:

$$\mathbf{c}_l(\mathbf{x}_n) = \hat{\mathbf{c}}_l(\mathbf{x}_n) = \mathcal{C}_l([\hat{\mathbf{x}}_i; \mathbf{x}_b]), \tag{C.21}$$

where \mathbf{v}_b is replaced by \mathbf{x}_b .

Proof of Eq.(3) From eq.(C.19), for any $[\hat{\mathbf{x}}_i; \mathbf{v}_b] \in \mathbb{R}^{m_{-1}} \times \mathbb{R}^M$, we define a sequence of matrices $\{\mathbf{J}_l([\hat{\mathbf{x}}_i; \mathbf{v}_b])\}_{l=0}^L$ by the recurrence relation:

$$\mathbf{J}_{0}([\hat{\mathbf{x}}_{i}; \mathbf{v}_{b}]) = [\mathbf{W}_{0}, \mathbf{R}_{0}] \in \mathbb{R}^{m_{0} \times (m_{-1} + M)},$$

$$\mathbf{J}_{l}([\hat{\mathbf{x}}_{i}; \mathbf{v}_{b}]) = \mathbf{W}_{l} \mathbf{\Sigma}_{l-1}([\hat{\mathbf{x}}_{i}; \mathbf{v}_{b}]) \mathbf{J}_{l-1}([\hat{\mathbf{x}}_{i}; \mathbf{v}_{b}]) + [\mathbf{O}_{l}, \mathbf{R}_{l}], 0 \leq l \leq L - 1$$

$$\mathbf{J}_{L}([\hat{\mathbf{x}}_{i}; \mathbf{v}_{b}]) = \mathbf{W}_{L} \mathbf{\Sigma}_{L-1}([\hat{\mathbf{x}}_{i}; \mathbf{v}_{b}]) \mathbf{J}_{L-1}([\hat{\mathbf{x}}_{i}; \mathbf{v}_{b}]) + [\mathbf{O}_{L}, \mathbf{R}_{L}],$$
(C.22)

where $[\cdot,\cdot]$ is an operator that concatenates two matrices; $\mathbf{R}_l \in \mathbb{R}^{m_t \times M}$ for $0 \le l \le L-1$, and $\mathbf{R}_L \in \mathbb{R}^{k \times M}$, is the matrix representations of the restriction operator \mathbf{r}_l ; $\mathbf{O}_l \in \mathbb{R}^{m_t \times m_{-1}}$ is a zero matrix; $\mathbf{\Sigma}_l([\hat{\mathbf{x}}_i; \mathbf{v}_b]) \in \mathbb{R}^{m_t \times m_t}$ is the Jacobian matrix of ReLU or Leaky ReLU in the l^{th} convolutional layer, which is precisely given by,

$$\Sigma_{l}([\hat{\mathbf{x}}_{i}; \mathbf{v}_{b}]) = diag\left(\frac{1+\gamma_{l}}{2} + \frac{1-\gamma_{l}}{2}sgn(\mathscr{C}_{l}([\hat{\mathbf{x}}_{i}; \mathbf{v}_{b}]))\right). \tag{C.23}$$

In fact, $\mathbf{J}_l([\hat{\mathbf{x}}_i; \mathbf{v}_b])$ is the Jacobian matrix of \mathscr{C}_l at $[\hat{\mathbf{x}}_i; \mathbf{v}_b]$. We point out that eq.(C.23) performs a hierarchal separation of the domain in the sense that, given a sequence of binary vectors $\mathbf{e} = \{e_l\}_{l=0}^L$ with $e_l \in \{-1, 1\}^{m_l}$ for $0 \le l \le L$, the Jacobian matrix \mathbf{J}_l shares on the same value on the subdomain $\Omega_l(\mathbf{e})$, where

$$\Omega_0(\mathbf{e}) = \mathbb{R}^{m_{-1}} \times \mathbb{R}^M,$$

$$\Omega_l(\mathbf{e}) = \{ [\hat{\mathbf{x}}_i; \mathbf{v}_b] \in \Omega_{l-1}(\mathbf{e}) : sgn(\mathscr{C}_{l-1}([\hat{\mathbf{x}}_i; \mathbf{v}_b])) = e_l \}, 0 \le l \le L.$$
(C.24)

As a direct consequence, for any $0 \le l \le L$ and $k \in \mathbb{R}^+$, we will have,

$$\mathbf{J}_l(k[\hat{\mathbf{x}}_i; \mathbf{v}_b]) = \mathbf{J}_l([\hat{\mathbf{x}}_i; \mathbf{v}_b]). \tag{C.25}$$

Note that $\mathbf{v}_b = \mathbf{x}_b$ is the case we discussed in Section 3.

With the above definitions, we can rewrite eq.(C.20) as,

$$\mathcal{C}_l([\hat{\mathbf{x}}_i; \mathbf{v}_b]) = \mathbf{J}_l([\hat{\mathbf{x}}_i; \mathbf{v}_b])[\hat{\mathbf{x}}_i; \mathbf{v}_b]. \tag{C.26}$$

Together with the fact that $\mathbf{J}_l([\hat{\mathbf{x}}_i; \mathbf{v}_b])$ is piecewise constant, eq.(C.26) reveals that \mathcal{C}_l is a piecewise linear function which passes through the origin in $\mathbb{R}^{m_{-1}+M}$. Furthermore, eq.(C.15), (C.17) can be rewritten as,

$$\mathbf{c}_{l}(\mathbf{x}_{n}) = \mathbf{J}_{l}(k[\hat{\mathbf{p}}_{-1}(\mathbf{x}_{n}); \mathbf{x}_{b}])[\hat{\mathbf{p}}_{-1}(\mathbf{x}_{n}); \mathbf{x}_{b}], 0 \le l \le L, k \in \mathbb{R}^{+}, \tag{C.27}$$

which proves the third equality in Eq.(3). For any piecewise linear activation function $\sigma(x)$, the following property holds,

$$\sigma(x_0) = x_0 \times \frac{d\sigma(x)}{x} \Big|_{x=x_0}, x_0 \in \mathbb{R}.$$
(C.28)

This implies that the proof works for any piecewise linear activation $\sigma(x)$ (whose derivative is piecewise constant) as long as we apply k = 1 and properly replace Σ_l in eq.(C.23) according to the selected $\sigma(x)$.

Appendix D Incorporating batch normalization (in detail)

In the l^{th} layer, the in-channel (in-ch) feature maps \mathbf{x}_{l-1} will convolve with the layer's kernels \mathbf{w}_l . The moving mean vector, μ , and moving variance vector, σ^2 , will normalize the convolved results before activating the layer's neuron. We summarize the BN computation below.

$$\mathbf{BN}(\mathbf{x}_{l-1}) = \gamma \times \frac{(\mathbf{x}_{l-1} \circledast \mathbf{w}_l - \mu)}{\sqrt{\sigma^2 + \epsilon}} + \beta, \tag{D.29}$$

where γ, β are two learnable parameters that weight feature maps channel-wise; a preset ϵ prevents any divide by zero exceptions (TensorFlow [27] sets $\epsilon = 0.001$). We can reduce its complexity using eq.(D.30) (fig.5),

$$\mathbf{BN}([\mathbf{x}_{l-1}; \mathbf{b}']) = \mathbf{x}_{l-1} \circledast \mathbf{w}_{l}' + \mathbf{b}'$$

$$\mathbf{w}_{l}' = \frac{(\gamma \times \mathbf{w}_{l})}{\sqrt{\sigma^{2} + \epsilon}}, \ \mathbf{b}' = (\beta - \frac{\gamma \times \mu}{\sqrt{\sigma^{2} + \epsilon}}). \tag{D.30}$$

It suggests that a CNN trained to use BNs is equivalent to a similar network graph illustrated in Fig.2 if \mathbf{w}_l and \mathbf{b}' are extracted from the trained CNN's batch normalization layer. Therefore, applying our theory to a CNN with BNs is as trivial as the first bias operational mode. Besides, eq.(D.30) significantly reduces both computations and DRAM consumption since fewer multiplications and parameters are required when compared to eq.(D.29). Note that this kind of transform is possible since we are dealing with a trained and fixed CNN.

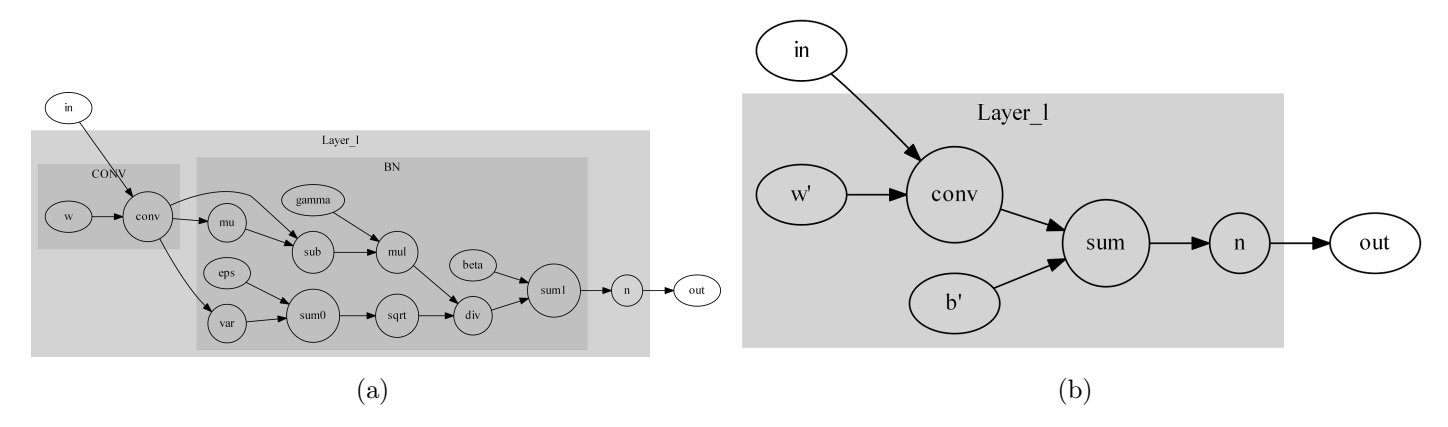


Figure 5: Batch normalization (BN) and its reduction. (a) A standard BN's implementation from eq.(D.29); (b) Reduction of BN to be compatible with our analysis (similar to Fig.2, via eq.(D.30)). Besides, this transformation lowers the computations and DRAM consumption.

Appendix E The algorithm and its implementation

The full algorithm is shown below in the next page (algorithm.1). Computing a jacobian is expensive, and we use convolution to accelerate our effective hypersurface reconstruction. Eq.(6) \sim (11) are optimized and compiled in algorithm.1. The paddings should be identical to those used during training. Tensorflow [27] functions matmul, unstack, stack, expanddim, conv2d, sum, are used in the algorithm. The transpose in Eq.(4) is achieved via an 'axis' option of the conv2d. From the algorithm we can see how the different reconstruction modes (RMs) are related.

Appendix F Histograms of relative errors

Histograms of relative errors between the CNN l^{th} layer's activation \mathbf{c}_l and the reconstructed counterpart $\hat{\mathbf{c}}_l$ on VGG7, ResNet20, and ResNet20-Fixup (10k test samples) are shown in fig.6, 7, and 8, respectively. Percentages of $\epsilon_l \leq 1\%$ collected from all subplots are listed in Table 2 in the main text. These results demonstrate the highly precise nature of our adjoint operator-based activity reconstruction approach.

Appendix G Tables

Algorithm 1: AdjointBackMapV2 with five modes $(RM_4 \text{ to } RM_0)$

return NULL

```
Input:
      1. x: input image (shape: d_1 = H \times W \times C);
      2. b: input bias vector concatenated from a trained model (shape: d_2);
      3. \mathbf{z}: the function for Eq.(3);
      4. \mathbf{F}_{l}: a forward mapping to in channels of the l^{th} laver;
      5. \mathbf{w}_l: the weights at the l^{th} layer;
      6. s: the convolution stride used during training
      7. M: RM to be used.
Output: Two parts of an effective hypersurface: \mathbf{H}^{Adj,I}(\mathbf{z}([\mathbf{x};\mathbf{b}])), \mathbf{H}^{Adj,b}(\mathbf{z}([\mathbf{x};\mathbf{b}]))
Function AdjointBackMap V2(\mathbf{x}, \mathbf{b}, \mathbf{z}, \mathbf{F}, \mathbf{w}_l, s, L):
       \mathbf{z}_0 = \mathbf{z}([\mathbf{x}; \mathbf{b}])
       if M is 'RM_0' then
               \begin{aligned} \mathbf{J_{F,x}}, & \mathbf{J_{F,b}}, \mathbf{J_{F,b}}, \mathbf{J_{F,b}}, \mathbf{J_{2}} \times c_{g_{\_}p,in} = \frac{\partial \mathbf{F}_{c_{g_{\_}p,in}}}{\partial \mathbf{x}}, \frac{\partial \mathbf{F}_{c_{g_{\_}p,in}}}{\partial \mathbf{b}} \\ & \mathbf{return} \ \mathrm{matmul}(\mathbf{J_{F,x}}, \mathbf{J_{1}} \times c_{g_{\_}p,in}(\mathbf{z_{0}}), \ \mathbf{w}_{fc, c_{g_{\_}p,in} \times c_{labels}}, \ \mathrm{axis=`} c_{g_{\_}p,in}'), \ \mathrm{matmul}(\mathbf{J_{F,b}}, \mathbf{J_{2}} \times c_{g_{\_}p,in}(\mathbf{z_{0}}), \mathbf{J_{2}}), \end{aligned}
                  \mathbf{w}_{fc,c_{g-p,in}\times c_{labels}}, \text{axis}='c_{g_{p,in}}'
       \mathbf{J}_{\mathbf{F},\mathbf{x},d_1\times h_l\times w_l\times c_{l,in}}, \mathbf{J}_{\mathbf{F},\mathbf{b},d_2\times h_l\times w_l\times c_{l,in}} = \frac{\partial \mathbf{F}_{h_l\times w_l\times c_{l,in}}}{\partial \mathbf{x}}, \frac{\partial \mathbf{F}_{h_l\times w_l\times c_{l,in}}}{\partial \mathbf{b}}
       switch M do
               case 'RM_4' or 'RM_3' do
                        \mathbf{w}_{r_1 \times r_2 \times c_{l,out}} = \operatorname{unstack}(\mathbf{w}_{l,r_1 \times r_2 \times c_{l,in} \times c_{l,out}}, \operatorname{axis=} c_{l,in})
                       \mathbf{J}_{\mathbf{F},\mathbf{x},d_1 \times h_l \times w_l} = \operatorname{unstack}(\mathbf{J}_{\mathbf{F},\mathbf{x},d_1 \times h_l \times w_l \times c_{l,in}}, \operatorname{axis=} c_{l,in})
                       \mathbf{J}_{\mathbf{F},\mathbf{b},d_2 \times h_l \times w_l} = \operatorname{unstack}(\mathbf{J}_{\mathbf{F},\mathbf{b},d_2 \times h_l \times w_l \times c_{l,in}}, \operatorname{axis=} c_{l,in})
                       j=0, Empty container R_x, R_b
                       while j < c_{l,in} do
                                \mathbf{J}_{\mathbf{F},\mathbf{x}} = \operatorname{expanddim}(\mathbf{J}_{\mathbf{F},\mathbf{x},d_1 \times h_l \times w_l}[j], \operatorname{axis='} c_{l,in}')
                                \mathbf{J}_{\mathbf{F},\mathbf{b}} = \operatorname{expanddim}(\mathbf{J}_{\mathbf{F},\mathbf{b},d_2 \times h_l \times w_l}[j], \operatorname{axis='} c_{l,in}')
                                \mathbf{w} = \operatorname{expanddim}(\mathbf{w}_{r_1 \times r_2 \times c_{l,out}}[j], \operatorname{axis}= c_{l,in})
                                R_x.append(conv2d(\mathbf{J}_{\mathbf{F},\mathbf{x}}(\mathbf{z}_0), \mathbf{w}, stride=s, axis='(h_l, w_l, c_{l,in}, c_{l,out})'))
                                R_b.append(conv2d(\mathbf{J_{F,b}}(\mathbf{z_0}), \mathbf{w}, stride=s, axis=(h_l, w_l, c_{l,in}, c_{l,out})'))
                               j = j + 1
                        \mathbf{H}_{I}, \mathbf{H}_{b} = \operatorname{stack}(R_{x}, \operatorname{axis}= c_{l,in}), \operatorname{stack}(R_{b}, \operatorname{axis}= c_{l,in})
                       if M is 'RM_4' then
                         \parallel return \mathbf{H}_I, \mathbf{H}_b
                        else if M is 'RM_3' then
                                return sum(\mathbf{H}_I, axis='(h_{l,o}, w_{l,o})'), sum(\mathbf{H}_b, axis='(h_{l,o}, w_{l,o})')
                case 'RM_2' or 'RM_1' do
                       \mathbf{H}_{I} = \operatorname{conv2d}(\mathbf{J}_{\mathbf{F},\mathbf{x},d_{1}\times h_{l}\times w_{l}\times c_{l,in}}(\mathbf{z}_{0}), \mathbf{w}_{l,r_{1}\times r_{2}\times c_{l,in}\times c_{l,out}}, \operatorname{stride}=s, \operatorname{axis}=`(h_{l}, w_{l}, c_{l,in}, c_{l,out})')
                       \mathbf{H}_b = \operatorname{conv2d}(\mathbf{J}_{\mathbf{F},\mathbf{b},d_2 \times h_l \times w_l \times c_{l,in}}(\mathbf{z}_0), \mathbf{w}_{l,r_1 \times r_2 \times c_{l,in} \times c_{l,out}}, \operatorname{stride}=s, \operatorname{axis}=`(h_l, w_l, c_{l,in}, c_{l,out})')
                       if M = 'RM_2' then
                         \lfloor return \mathbf{H}_I, \mathbf{H}_b
                        else if M = RM_1 then
                               return sum(\mathbf{H}_I, axis='(h_{l,o}, w_{l,o})'), sum((\mathbf{H}_b, axis='(h_{l,o}, w_{l,o})')
```

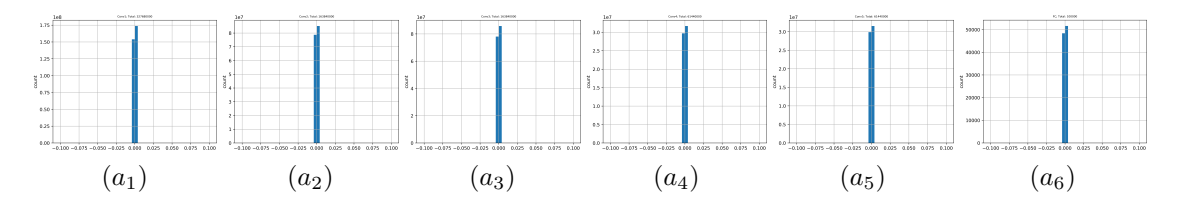


Figure 6: Histograms of relative errors between \mathbf{c}_l and $\hat{\mathbf{c}}_l$ (Eq.(14)) on VGG7. The x-axis and y-axis indicate the error and frequency (10k test samples), respectively. $a_1 \sim a_5$ is collected from conv1 ~ 5 layer, and a_6 is collected from the FC layer. In terms of the 4^{th} column of table.3, a_1 to a_6 should have quantities of relative errors: $327.68m(=32,768\times10k), 163.84m(=16,384\times10k), 163.84m, 61.44m(=6,144\times10k), 61.44m, 100k$, respectively, which has been numerically confirmed in its title as well. Percentages of $\epsilon_l \leq 1\%$ for all subplots are listed in Table 2.

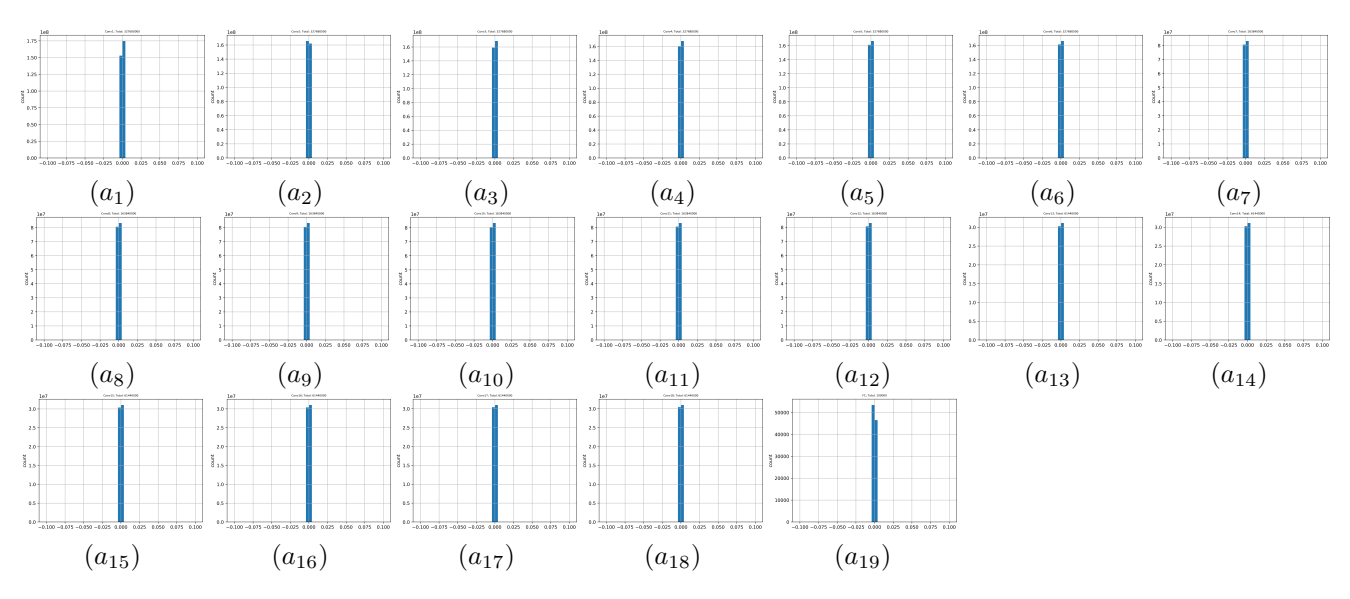


Figure 7: Histograms of relative errors between \mathbf{c}_l and $\hat{\mathbf{c}}_l$ (Eq.(14)) on ResNet20. Similar to fig.6, $a_1 \sim a_{18}$ is collected from conv1 \sim 18 layer, and a_{19} is collected from the FC layer. In terms of the 5th column of table.5, a_1 to a_{18} should have quantities of relative errors: $327.68m(a_1 \sim a_6)$, $163.84m(a_7 \sim a_{12})$, $61.44m(a_{13} \sim a_{18})$, $100k(a_{19})$, respectively, and also has been numerically confirmed as its title. Percentages of $\epsilon_l \leq 1\%$ for all subplots are listed in Table 2.

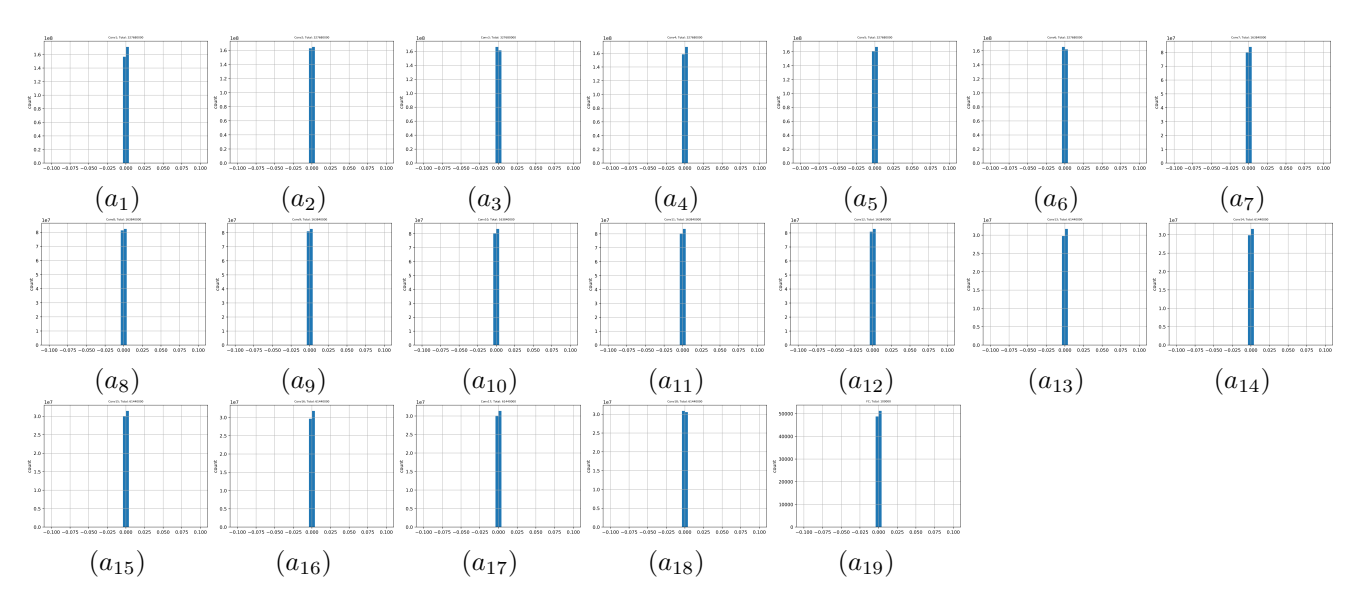


Figure 8: Histograms of relative errors between \mathbf{c}_l and $\hat{\mathbf{c}}_l$ (ϵ , Eq.(14)) on ResNet20-Fixup. Details are similar to fig.7. Percentages of $\epsilon_l \leq 1\%$ for all subplots are listed in Table 2.

Table 3: Parameters for VGG7.

Original Layer Equivalent Layer		Parameters	Out-ch Feature Maps	
Input (\mathbf{x}_n)	Input $([\mathbf{x}_n; \mathbf{x}_b])$	N/A	N/A	
$Conv0 (\mathbf{w}_0)$	$Conv0 (\mathbf{w}_0')$	N/A	N/A	
BN0	$B0 (\mathbf{x}_b[\mathbf{b}_0'])$	N/A	N/A	
Re	eLU0	N/A	N/A	
Conv1 (\mathbf{w}_1)	$Conv1 (\mathbf{w}_1')$	$3 \times 3 \times 32 \times 32$	$32 \times 32 \times 32 (= 32,768)$	
BN1	$\mathrm{B1}\;(\mathbf{x}_b[\mathbf{b}_1^{'}])$	N/A	N/A	
	eLU1	N/A	N/A	
Avg	-pool-2	N/A	N/A	
$Conv2 (\mathbf{w}_2)$	$Conv2 (\mathbf{w}_{2}')$	$3 \times 3 \times 32 \times 64$	$16 \times 16 \times 64 (= 16, 384)$	
BN2	$\mathrm{B2}\;(\mathbf{x}_b[\mathbf{b}_2^{'}])$	N/A	$\mathrm{N/A}$	
Re	eLU2	N/A	N/A	
Conv3 (\mathbf{w}_3)	$Conv3 (\mathbf{w}_{3}')$	$3 \times 3 \times 64 \times 64$	$16 \times 16 \times 64 (= 16, 384)$	
BN3	$B3 (\mathbf{x}_b[\mathbf{b}_3'])$	N/A	$\mathrm{N/A}$	
Re	eLU3	N/A	N/A	
Avg	-pool-2	N/A	N/A	
$Conv4$ (\mathbf{w}_4)	$Conv4 (\mathbf{w}_{4}^{'})$	$3 \times 3 \times 64 \times 96$	$8 \times 8 \times 96 (= 6, 144)$	
BN4	$B4 (\mathbf{x}_b[\mathbf{b}_4'])$	N/A	$\mathrm{N/A}$	
Re	eLU4	N/A	N/A	
Conv5 (\mathbf{w}_5)	$Conv5 (\mathbf{w}_{5}')$	$3 \times 3 \times 96 \times 96$	$8 \times 8 \times 96 (= 6, 144)$	
BN5	$B5 (\mathbf{x}_b[\mathbf{b}_5'])$	N/A	$\mathrm{N/A}$	
ReLU5		N/A	N/A	
global-pool (g_p)		N/A	N/A	
$FC (\mathbf{w}_{fc})$		96×10	10	
ReLU6		N/A	$\mathrm{N/A}$	

 $[\]mathbf{w}_{i}^{'}$ and $\mathbf{b}_{i}^{'}$ are computed using eq.(D.30); \mathbf{x}_{b} is a sequentical concatenation of $\mathbf{b}_{0}^{'} \sim \mathbf{b}_{5}^{'}$;

Table 4: Dimensions of $\mathbf{H}^{Adj}(\frac{[\mathbf{x}_n;\mathbf{x}_b]}{8})$ with different RMs On VGG7.

		\ 8 /			
Equivalent Layer	RM_4	RM_3	RM_2	RM_1	RM_0
Conv0	N/A	N/A	N/A	N/A	N/A
Conv1	$d_{in} \times 32 \times 32 \times 32 \times 32$	$d_{in} \times 32 \times 32$	$d_{in} \times 32 \times 32 \times 32$	$d_{in} \times 32$	N/A
Conv2	$d_{in} \times 16 \times 16 \times 32 \times 64$	$d_{in} \times 32 \times 64$	$d_{in} \times 16 \times 16 \times 64$	$d_{in} \times 64$	N/A
Conv3	$d_{in} \times 16 \times 16 \times 64 \times 64$	$d_{in} \times 64 \times 64$	$d_{in} \times 16 \times 16 \times 64$	$d_{in} \times 64$	N/A
Conv4	$d_{in} \times 8 \times 8 \times 64 \times 96$	$d_{in} \times 64 \times 96$	$d_{in} \times 8 \times 8 \times 96$	$d_{in} \times 96$	N/A
Conv5	$d_{in} \times 8 \times 8 \times 96 \times 96$	$d_{in} \times 96 \times 96$	$d_{in} \times 8 \times 8 \times 96$	$d_{in} \times 96$	N/A
FC	N/A	N/A	N/A	N/A	$d_{in} \times 10$

 $d_{in} = (32 \times 32 \times 3 + 384)$ where $384 = (32 + 64 + 96) \times 2$;

N/A: it is not necessary for our method.

Avg-pool-2: average pooling with window size of 3 and stride of 2;

N/A: it is not necessary for our method.

Table 5: Parameters for ResNet20 (refer to table 3).

		ters for ResNet20 (
Block (shortcut)	Original layer	Equivalent layer	Parameters	Out-ch feature map
	Input (\mathbf{x}_n)	Input $([\mathbf{x}_n; \mathbf{x}_b])$	N/A	N/A
	Conv0 (\mathbf{w}_0)	$Conv0$ $(\mathbf{w}_{0}^{'})$	N/A	N/A
	BN0	B0 $(\mathbf{x}_b[\mathbf{b}_0'])$	N/A	N/A
	Leaky	_ReLU0	N/A	N/A
Residual 0	Conv1 (\mathbf{w}_1)	Conv1 (\mathbf{w}_1')	$3 \times 3 \times 32 \times 32$	$32 \times 32 \times 32(32,768)$
(identity)	BN1	B1 $(\mathbf{x}_b[\mathbf{b}_1])$	N/A	N/A
	Leaky	_ReLU1	N/A	N/A
	Conv2 (\mathbf{w}_2)	$Conv2 (\mathbf{w}_{2}')$	$3 \times 3 \times 32 \times 32$	$32 \times 32 \times 32(32,768)$
	BN2	B2 $(\mathbf{x}_b[\mathbf{b}_2])$	N/A	N/A
	Leaky		N/A	N/A
Residual 1	Conv3 (\mathbf{w}_3)	$Conv3 (\mathbf{w}_3)$	$3 \times 3 \times 32 \times 32$	$32 \times 32 \times 32(32,768)$
(identity)	BN3	$B3 \left(\mathbf{x}_b [\mathbf{b}_3'] \right)$	N/A	N/A
	Leaky		N/A	N/A
	Conv4 (\mathbf{w}_4)	$Conv4 (\mathbf{w}_{4}')$	$3 \times 3 \times 32 \times 32$	$32 \times 32 \times 32(32,768)$
	BN4	$B4 \left(\mathbf{x}_b[\mathbf{b}_4']\right)$	N/A	N/A
	Leaky		N/A	N/A
Residual 2	Conv5 (\mathbf{w}_5)	Conv5 (\mathbf{w}_{5}')	$3 \times 3 \times 32 \times 32$	$32 \times 32 \times 32(32,768)$
(identity)	BN5	$B5 \left(\mathbf{x}_b[\mathbf{b}_5']\right)$	N/A	N/A
	Leaky		N/A	N/A
	Conv6 (\mathbf{w}_6)	Conv6 (\mathbf{w}_{6}')	$3 \times 3 \times 32 \times 32$	$32 \times 32 \times 32(32,768)$
	BN6	$B6 (\mathbf{x}_b[\mathbf{b}_6'])$	N/A	N/A
		ReLU6	N/A	N/A
Residual 3	$Conv7 (\mathbf{w}_7, s = 2)$	Conv7 ($\mathbf{w}_{7}', s = 2$)	$3 \times 3 \times 32 \times 64$	$16 \times 16 \times 64 (16, 384)$
(avg-pool+pad)	BN7	$B7 (\mathbf{x}_b[\mathbf{b}_7'])$	N/A	N/A
	Leaky		N/A	N/A
	Conv8 (\mathbf{w}_8)	Conv8 (\mathbf{w}_8')	$3 \times 3 \times 64 \times 64$	$16 \times 16 \times 64(16, 384)$
	BN8	$B8 \left(\mathbf{x}_b[\mathbf{b}_8']\right)$	N/A	N/A
		ReLU8	N/A	N/A
Residual 4	Conv9 (\mathbf{w}_9)	Conv9 (\mathbf{w}_9')	$3 \times 3 \times 64 \times 64$	$16 \times 16 \times 64(16, 384)$
(identity)	BN9	$B9 (\mathbf{x}_b[\mathbf{b}_0'])$	N/A	N/A
, , , , ,		ReLU9	N/A	N/A
	Conv10 (\mathbf{w}_{10})	Conv10 (\mathbf{w}'_{10})	$3 \times 3 \times 64 \times 64$	$16 \times 16 \times 64(16, 384)$
	BN10	B10 $(\mathbf{x}_b[\mathbf{b}'_{10}])$	N/A	N/A
		ReLU10	N/A	N/A
Residual 5	Conv11 (\mathbf{w}_{11})	Conv11 (\mathbf{w}'_{11})	$3 \times 3 \times 64 \times 64$	$16 \times 16 \times 64(16, 384)$
(identity)	BN11	B11 $(\mathbf{x}_b[\mathbf{b}'_{11}])$	N/A	N/A
, , , , ,		ReLU11	N/A	N/A
	Conv12 (\mathbf{w}_{12})	Conv12 $(\mathbf{w}_{12}^{'})$	$3 \times 3 \times 64 \times 64$	$16 \times 16 \times 64(16, 384)$
	BN12	$B12 \left(\mathbf{x}_{b}[\mathbf{b}_{12}^{'}]\right)$	N/A	N/A
		ReLU12	N/A	N/A
Residual 6	Conv13 ($\mathbf{w}_{13}, s = 2$)		$3 \times 3 \times 64 \times 96$	$8 \times 8 \times 96(6, 144)$
(avg-pool+pad)	BN13	$\frac{\text{B13 } (\mathbf{x}_b[\mathbf{b}'_{13}])}{\text{B13 } (\mathbf{x}_b[\mathbf{b}'_{13}])}$	N/A	N/A
`		ReLU13	N/A	N/A
	Conv14 (\mathbf{w}_{14})	Conv14 (w ₁₄)	$3 \times 3 \times 96 \times 96$	$8 \times 8 \times 96(6, 144)$
	BN14	$B14 (\mathbf{x}_{b}[\mathbf{b}'_{14}])$	N/A	N/A
		ReLU14	N/A	N/A
Residual 7	Conv15 (\mathbf{w}_{15})	$\frac{\text{Conv15 } (\mathbf{w}_{15}')}{\text{Conv15 } (\mathbf{w}_{15}')}$	$3 \times 3 \times 96 \times 96$	$8 \times 8 \times 96(6, 144)$
(identity)	BN15	$B15 \left(\mathbf{x}_{b}[\mathbf{b}_{15}^{'}]\right)$	N/A	N/A
` ' '	Leaky_	ReLU15	N/A N/A	N/A N/A
	$\frac{\text{Conv16 } (\mathbf{w}_{16})}{\text{Conv16 } (\mathbf{w}_{16})}$	$\frac{\text{Conv16 } (\mathbf{w}_{16}')}{\text{Conv16 } (\mathbf{w}_{16}')}$	$3 \times 3 \times 96 \times 96$	$8 \times 8 \times 96(6, 144)$
	BN16	$\frac{\text{B16 } (\mathbf{x}_b[\mathbf{b}'_{16}])}{\text{B16 } (\mathbf{x}_b[\mathbf{b}'_{16}])}$	N/A	N/A
		ReLU16	N/A N/A	N/A N/A
Residual 8	$\frac{\text{Conv17 } (\mathbf{w}_{17})}{\text{Conv17 } (\mathbf{w}_{17})}$	$\frac{\text{Conv17 } (\mathbf{w}_{17}^{'})}{\text{Conv17 } (\mathbf{w}_{17}^{'})}$	$3 \times 3 \times 96 \times 96$	$8 \times 8 \times 96(6, 144)$
(identity)	BN17	$\frac{\text{B17}\left(\mathbf{x}_{b}[\mathbf{b}_{17}^{'}]\right)}{\text{B27}\left(\mathbf{x}_{b}[\mathbf{b}_{17}^{'}]\right)}$	N/A	N/A
($\frac{\text{B1} t \left(\mathbf{x}_{b}[\mathbf{b}_{17}]\right)}{\text{ReLU17}}$	N/A N/A	N/A N/A
	Conv18 (\mathbf{w}_{18})	Conv18 (\mathbf{w}_{18}')	$3 \times 3 \times 96 \times 96$	$8 \times 8 \times 96(6, 144)$
	BN18		N/A	N/A
		$\begin{array}{ c c c c }\hline B18 & (\mathbf{x}_b[\mathbf{b}_{18}]) \\ \hline ReLU18 & \end{array}$	N/A N/A	N/A N/A
	· -	-	N/A N/A	N/A N/A
		\mathbf{p} (\mathbf{w}_{fc})	96×10	10
		. we to !	ı ∂U ∧ 1U	10
		ReLU19	N/A	N/A

 \mathbf{x}_b is a sequentical concatenation of $\mathbf{b}_0' \sim \mathbf{b}_{18}'$; avg-pool: average pooling with window size of 1 and stride of 2;

pad: padding zero channels to match the quantity of out-channels for summation.

Table 6: Parameters for ResNet20-Fixup (refer to table 5)

Table 6		ior ResNet20-	- \	
Block (shortcut)	Original layer	Equivalent layer	Parameters	Out-channel feature map
	Input (\mathbf{x}_n)	Input $([\mathbf{x}_n; \mathbf{x}_b])$	N/A	N/A N/A
	$Conv0$ (\mathbf{w}_0) $B0$ (b_0)	Conv0 (\mathbf{w}_0) B0 ($\mathbf{x}_b[b_0]$)	N/A N/A	N/A N/A
		LU0	N/A N/A	N/A N/A
Residual 0	B1 (b ₁)	B1 $(\mathbf{x}_b[b_1])$	N/A	N/A
(identity)	Conv1 (\mathbf{w}_1)	Conv1 (\mathbf{w}_1)	$3 \times 3 \times 32 \times 32$	$32 \times 32 \times 32(32,768)$
	B2 (b2)	B2 $(\mathbf{x}_b[b_2])$	N/A	N/A
		LU1	N/A	N/A
	B3 (b_3)	B3 $(\mathbf{x}_b[b_3])$	N/A	N/A
	Conv2 (\mathbf{w}_2)	Conv2	$3 \times 3 \times 32 \times 32$	$32 \times 32 \times 32(32,768)$
	$M2 (M_2)$	$(\mathbf{w}_{2}^{'} = \mathbf{w}_{2} \times M_{2})$		
	B4 (b ₄)	B4 $(\mathbf{x}_b[b_4])$	N/A	N/A
Residual 1	B5 (b ₅)	$\begin{array}{ c c c } \text{LU2} \\ \hline & \text{B5 } (\mathbf{x}_b[b_5]) \end{array}$	N/A N/A	N/A N/A
(identity)	$Conv3$ (\mathbf{w}_3)	Conv3 (\mathbf{w}_3)	$3 \times 3 \times 32 \times 32$	$32 \times 32 \times 32(32,768)$
(B6 (b ₆)	$B6 (\mathbf{x}_b[b_6])$	N/A	N/A
		LU3	N/A	N/A
	B7 (b_7)	B7 $(\mathbf{x}_b[b_7])$	N/A	N/A
	Conv4 (\mathbf{w}_4)	Conv4	$3 \times 3 \times 32 \times 32$	$32 \times 32 \times 32(32,768)$
	M4 (M ₄)	$(\mathbf{w}_{4}^{'} = \mathbf{w}_{4} \times M_{4})$		
	B8 (b ₈)	B8 $(\mathbf{x}_b[b_8])$	N/A	N/A
D 1 - 1 0		LU4	N/A	N/A
Residual 2 (identity)	$B9 (b_9)$ $Conv5 (\mathbf{w}_5)$	B9 $(\mathbf{x}_b[b_9])$ Conv5 (\mathbf{w}_5)	N/A $3 \times 3 \times 32 \times 32$	N/A $32 \times 32 \times 32(32,768)$
(recitatey)	B10 (b ₁₀)	B10 $(\mathbf{x}_b[b_{10}])$	N/A	N/A
		LU5	N/A	N/A
ŀ	B11 (b ₁₁)	B11 $(\mathbf{x}_b[b_{11}])$	N/A	N/A
ŀ	Conv6 (\mathbf{w}_6)	Conv6		,
ľ	M6 (M_6)	$({\bf w}_{6}' = {\bf w}_{6} \times M_{6})$	$3 \times 3 \times 32 \times 32$	$32 \times 32 \times 32(32,768)$
	B12 (b_{12})	B12 $(\mathbf{x}_b[b_{12}])$	N/A	N/A
		LU6	N/A	N/A
Residual 3	B13 (b ₁₃)	B13 $(\mathbf{x}_b[b_{13}])$	N/A	N/A
(avg-pool+pad)	$Conv7 (\mathbf{w}_7, s = 2)$	$Conv7 (\mathbf{w}_7, s = 2)$	$3 \times 3 \times 32 \times 64$	$16 \times 16 \times 64(16, 384)$
	B14 (b ₁₄)	B14 $(\mathbf{x}_b[b_{14}])$ LU7	N/A N/A	N/A N/A
	B15 (b ₁₅)	B15 $(\mathbf{x}_{b}[b_{15}])$	N/A N/A	N/A N/A
•	Conv8 (w ₈)	Conv8	· ·	,
	M8 (M ₈)	$(\mathbf{w}_{8}' = \mathbf{w}_{8} \times M_{8})$	$3 \times 3 \times 64 \times 64$	$16 \times 16 \times 64(16, 384)$
	B16 (b ₁₆)	B16 $(\mathbf{x}_{b}[b_{16}])$	N/A	N/A
		LU8	N/A	N/A
Residual 4	B17 (b_{17})	B17 $(\mathbf{x}_b[b_{17}])$	N/A	N/A
(identity)	Conv9 (\mathbf{w}_9)	Conv9 (\mathbf{w}_9)	$3 \times 3 \times 64 \times 64$	$16 \times 16 \times 64(16, 384)$
	B18 (b_{18})	B18 $(\mathbf{x}_b[b_{18}])$	N/A	N/A
		LU9	N/A	N/A
	$B19 (b_{19})$ $Conv10 (\mathbf{w}_{10})$	$B19 (\mathbf{x}_b[b_{19}])$ Conv10	N/A	N/A
	$M10 (M_{10})$	$(\mathbf{w}_{10}^{'} = \mathbf{w}_{10} \times M_{10})$	$3 \times 3 \times 64 \times 64$	$16 \times 16 \times 64(16, 384)$
	B20 (b ₂₀)	$B20 \ (\mathbf{x}_b[b_{20}])$	N/A	N/A
		U10	N/A	N/A
Residual 5	B21 (b ₂₁)	B21 $(\mathbf{x}_b[b_{21}])$	N/A	N/A
(identity)	Conv11 (\mathbf{w}_{11})	Conv11 (\mathbf{w}_{11})	$3 \times 3 \times 64 \times 64$	$16 \times 16 \times 64(16, 384)$
	B22 (b_{22})	B22 $(\mathbf{x}_b[b_{22}])$	N/A	N/A
	ReL		N/A	N/A
	B23 (b ₂₃)	$B23 (\mathbf{x}_b[b_{23}])$	N/A	N/A
	Conv12 (\mathbf{w}_{12}) M12 (M_{12})	Conv12 $(\mathbf{w}'_{12} = \mathbf{w}_{12} \times M_{12})$	$3 \times 3 \times 64 \times 64$	$16 \times 16 \times 64(16, 384)$
	B24 (b ₂₄)	$(\mathbf{w}_{12} - \mathbf{w}_{12} \times M_{12})$ $B24 (\mathbf{x}_b[b_{24}])$	N/A	N/A
		U12	N/A N/A	N/A N/A
Residual 6	B25 (b ₂₅)	B25 $(\mathbf{x}_b[b_{25}])$	N/A	N/A
(avg-pool+pad)	Conv13 ($\mathbf{w}_{13}, s = 2$)		$3 \times 3 \times 64 \times 96$	8 × 8 × 96(6, 144)
- /	B26 (b ₂₆)	$B26 \ (\mathbf{x}_b[b_{26}])$	N/A	N/A
	ReL	U13	N/A	N/A
	B27 (b_{27})	$B27 (\mathbf{x}_b[b_{27}])$	N/A	N/A
[Conv14 (w ₁₄)	Conv14	$3 \times 3 \times 96 \times 96$	$8 \times 8 \times 96(6, 144)$
	M14 (M ₁₄)	$(\mathbf{w}_{14} = \mathbf{w}_{14} \times M_{14})$		` ' '
	B28 (b ₂₈)	B28 $(\mathbf{x}_b[b_{28}])$ JU14	N/A N/A	N/A N/A
Residual 7	B29 (b ₂₉)	$B29 (\mathbf{x}_b[b_{29}])$	N/A N/A	N/A N/A
(identity)	Conv15 (\mathbf{w}_{15})	Conv15 (\mathbf{w}_{15})	$3 \times 3 \times 96 \times 96$	8 × 8 × 96(6, 144)
` "/	B30 (b ₃₀)	$B30 (\mathbf{x}_b[b_{30}])$	N/A	N/A
ļ	ReL	U15	N/A	N/A
	B31 (b_{31})	B31 $(\mathbf{x}_b[b_{31}])$	N/A	N/A
	Conv16 (\mathbf{w}_{16})	Conv16	$3 \times 3 \times 96 \times 96$	$8 \times 8 \times 96(6, 144)$
[M16 (M ₁₆)	$(\mathbf{w}_{16}^{'} = \mathbf{w}_{16} \times M_{16})$		
	B32 (b ₃₂)	B32 $(\mathbf{x}_b[b_{32}])$.U16	N/A	N/A N/A
Residual 8			N/A	N/A
Residual 8 (identity)	$B33 (b_{33})$ Conv16 (w ₁₆)	B33 $(\mathbf{x}_b[b_{33}])$ Conv16 (\mathbf{w}_{16})	N/A $3 \times 3 \times 96 \times 96$	N/A 8 × 8 × 96(6, 144)
(B34 (b ₃₄)	$B34 (\mathbf{x}_b[b_{34}])$	N/A	N/A
ŀ		U17	N/A N/A	N/A N/A
l l	B35 (b ₃₅)	$B35 (\mathbf{x}_{b}[b_{35}])$	N/A	N/A
l	Conv18 (w ₁₈)	Conv18		
		$(\mathbf{w}_{18}^{'} = \mathbf{w}_{18} \times M_{18})$	$3 \times 3 \times 96 \times 96$	$8 \times 8 \times 96(6, 144)$
	$M18 (M_{18})$			37/4
	B36 (b_{36})	B36 $(\mathbf{x}_b[b_{36}])$	N/A	N/A
	B36 (b ₃₆) ReI	B36 $(\mathbf{x}_b[b_{36}])$.U18	N/A	N/A
	B36 (b ₃₆) ReL	$B36 (\mathbf{x}_b[b_{36}])$ $U18$ _P	N/A N/A	N/A N/A
	B36 (b ₃₆) ReI g FC (B36 $(\mathbf{x}_b[b_{36}])$.U18	N/A	N/A

 M_i denotes a multiplier [31]; \mathbf{x}_b is a sequentical concatenation of $b_0 \sim b_{36}$.

Table 7: Dimensions of $\mathbf{H}^{Adj}(\frac{[\mathbf{x}_n;\mathbf{x}_b]}{8})$ with different RMs on ResNet20/ResNet20-Fixup.

Equivalent layer	RM_4	RM_3	RM_2	RM_1	RM_0
Conv0	N/A	N/A	N/A	N/A	N/A
Conv1	$d_{in} \times 32 \times 32 \times 32 \times 32$	$d_{in} \times 32 \times 32$	$d_{in} \times 32 \times 32 \times 32$	$d_{in} \times 32$	N/A
Conv2	$d_{in} \times 32 \times 32 \times 32 \times 32$	$d_{in} \times 32 \times 32$	$d_{in} \times 32 \times 32 \times 32$	$d_{in} \times 32$	N/A
Conv3	$d_{in} \times 32 \times 32 \times 32 \times 32$	$d_{in} \times 32 \times 32$	$d_{in} \times 32 \times 32 \times 32$	$d_{in} \times 32$	N/A
Conv4	$d_{in} \times 32 \times 32 \times 32 \times 32$	$d_{in} \times 32 \times 32$	$d_{in} \times 32 \times 32 \times 32$	$d_{in} \times 32$	N/A
Conv5	$d_{in} \times 32 \times 32 \times 32 \times 32$	$d_{in} \times 32 \times 32$	$d_{in} \times 32 \times 32 \times 32$	$d_{in} \times 32$	N/A
Conv6	$d_{in} \times 32 \times 32 \times 32 \times 32$	$d_{in} \times 32 \times 32$	$d_{in} \times 32 \times 32 \times 32$	$d_{in} \times 32$	N/A
Conv7	$d_{in} \times 16 \times 16 \times 32 \times 64$	$d_{in} \times 32 \times 64$	$d_{in} \times 16 \times 16 \times 64$	$d_{in} \times 64$	N/A
Conv8	$d_{in} \times 16 \times 16 \times 64 \times 64$	$d_{in} \times 64 \times 64$	$d_{in} \times 16 \times 16 \times 64$	$d_{in} \times 64$	N/A
Conv9	$d_{in} \times 16 \times 16 \times 64 \times 64$	$d_{in} \times 64 \times 64$	$d_{in} \times 16 \times 16 \times 64$	$d_{in} \times 64$	N/A
Conv10	$d_{in} \times 16 \times 16 \times 64 \times 64$	$d_{in} \times 64 \times 64$	$d_{in} \times 16 \times 16 \times 64$	$d_{in} \times 64$	N/A
Conv11	$d_{in} \times 16 \times 16 \times 64 \times 64$	$d_{in} \times 64 \times 64$	$d_{in} \times 16 \times 16 \times 64$	$d_{in} \times 64$	N/A
Conv12	$d_{in} \times 16 \times 16 \times 64 \times 64$	$d_{in} \times 64 \times 64$	$d_{in} \times 16 \times 16 \times 64$	$d_{in} \times 64$	N/A
Conv13	$d_{in} \times 8 \times 8 \times 64 \times 96$	$d_{in} \times 64 \times 96$	$d_{in} \times 8 \times 8 \times 96$	$d_{in} \times 96$	N/A
Conv14	$d_{in} \times 8 \times 8 \times 96 \times 96$	$d_{in} \times 96 \times 96$	$d_{in} \times 8 \times 8 \times 96$	$d_{in} \times 96$	N/A
Conv15	$d_{in} \times 8 \times 8 \times 96 \times 96$	$d_{in} \times 96 \times 96$	$d_{in} \times 8 \times 8 \times 96$	$d_{in} \times 96$	N/A
Conv16	$d_{in} \times 8 \times 8 \times 96 \times 96$	$d_{in} \times 96 \times 96$	$d_{in} \times 8 \times 8 \times 96$	$d_{in} \times 96$	N/A
Conv17	$d_{in} \times 8 \times 8 \times 96 \times 96$	$d_{in} \times 96 \times 96$	$d_{in} \times 8 \times 8 \times 96$	$d_{in} \times 96$	N/A
Conv18	$d_{in} \times 8 \times 8 \times 96 \times 96$	$d_{in} \times 96 \times 96$	$d_{in} \times 8 \times 8 \times 96$	$d_{in} \times 96$	N/A
FC	N/A	N/A	N/A	N/A	$d_{in} \times 10$

For ResNet20: $d_{in} = (32 \times 32 \times 3 + 1, 152)$ where $1, 152 = (32 + 64 + 96) \times 6$; For ResNet20-Fixup: $d_{in} = (32 \times 32 \times 3 + 37)$.